bioRxiv preprint doi: https://doi.org/10.1101/498980; this version posted December 17, 2018. The copyright holder for this preprint (which was not certified by peer review) is the author/funder. All rights reserved. No reuse allowed without permission.

Novel mechanisms of bone cancer pain revealed with in vivo GCaMP6s imaging

Mateusz W. Kucharczyk[1, 2, 3, 4, *], Kim I. Chisholm[2], Douglas M. Lopes[2], Diane Derrien[1], Franziska Denk[2], Kirsty Bannister[3], Anthony H. Dickenson[1], Stephen B. McMahon[2]

[1]Department of Neuroscience, Physiology and Pharmacology, University College London, Gower Street, WC1E 6BT London, UK

[2]Neurorestoration Group, Wolfson Centre for Age-Related Diseases, King's College London, London SE1 1UL, UK

[3]Central Modulation of Pain Group, Wolfson Centre for Age-Related Diseases, King's College London, London SE1 1UL, UK

[4]Lead contact

*Correspondence:
mateusz.kucharczyk@kcl.ac.uk
matwku@gmail.com
Neurorestoration Group,
Wolfson Centre for Age-Related Diseases,
King's College London,
London SE1 1UL, UK

bioRxiv preprint doi: https://doi.org/10.1101/498980; this version posted December 17, 2018. The copyright holder for this preprint (which was not certified by peer review) is the author/funder. All rights reserved. No reuse allowed without permission.

Abstract

Cancer pain remains a major area of unmet medical need, with few studies existing in proportion to that need. One common form, affecting 400,000 people each year in the US alone, is associated with skeletal metastases. These pains are typically mechanoceptive in nature and poorly managed by available analgesics. Here, we employed *in vivo* imaging using GCaMP6s to assess the properties of the nerve fibres that convey bone cancer pains. We find that a subclass of nociceptors, those that are normally mechanically insensitive, are recruited and activated in a rodent model of bone cancer, and this dramatically increases sensory input from the diseased tissue to the central nervous system. The recruitment of these so-called silent afferents was found to be Piezo2-dependent. The unique properties of these silent afferents offer several novel opportunities for targeting metastatic bone pain.

Keywords

Cancer-induced bone pain; Silent nociceptors; Sensory coding; Pressure cuff; Mechanosensitive pain; In vivo calcium imaging; Tissue clearing; Piezo2; Advillin.

bioRxiv preprint doi: https://doi.org/10.1101/498980; this version posted December 17, 2018. The copyright holder for this preprint (which was not certified by peer review) is the author/funder. All rights reserved. No reuse allowed without permission.

Introduction

Following a cancer diagnosis, patients must deal with a range of unpleasantries resulting not only from cancer growth but also from treatment. A significant side effect of certain cancer types is severe pain, which can persist even in remission[1–3].

Cancer pain is particularly prominent in cases where malignant tumours have invaded the skeleton[2,4]. Neurologists broadly classify pain into two types: nociceptive (sharp, throbbing; stimulus driven) and neuropathic (abnormal sensations due to nervous system damage)[3]. Cancer-induced bone pain (CIBP) is a unique mix of both, with sufferers experiencing tonic, spontaneous and movement-evoked pain. The latter is also known as “break-through” or suprathreshold pain. This type of pain, being mechanoceptive in nature, is difficult to manage in mobile subjects, as by definition, it ‘breaks-through’ the barriers of analgesia[3].

Mechanistically, CIBP is transmitted via peripheral sensory neurons, the cell bodies of which are housed in discrete dorsal root ganglia (DRG) buried deep underneath the spinal cord vertebrae. These pseudounipolar cells transmit nociceptive information from the tumour environment in the bone to the dorsal horn of the spinal cord. From there, the nociceptive signal is relayed to various brain regions.

Over the past decade, rodent studies of CIBP have revealed that neurons and cancer cells are engaged in bi-directional crosstalk. For instance, cancer causes a reorganization of normal anatomy, driving neurons to sprout and more densely innervate the tumour-bearing bone[2,5,6]. This sprouting process is mediated via tyrosine kinase A (TrkA) receptor activation by nerve growth factor (NGF) released from both cancer and stromal cells[7–9]. Conversely, neurons release factors which support tumour growth and vascularization[10–12]. This complex dialogue involves numerous mediators and different local cells, including fibroblasts, osteoclasts and newly recruited immune cells[3,10].

Despite pioneering work, many questions remain regarding bone afferent function, both in health and disease. For instance, do they encode mechanical stimuli, and if so, how? And, most importantly, how are their functional responses altered in cancer conditions? This study was designed to address these outstanding questions using cell-type specific molecular approaches together with *in vivo*

bioRxiv preprint doi: https://doi.org/10.1101/498980; this version posted December 17, 2018. The copyright holder for this preprint (which was not certified by peer review) is the author/funder. All rights reserved. No reuse allowed without permission.

functional imaging. We utilised an animal model of breast cancer metastasis to study CIBP. The model is recognised as having high face and construct validity compared to its human counterpart[3].

The data gathered reveal important new information about bone afferent expression patterns, encoding of mechanical stimuli and potential functional mechanism explaining hyperexcitablity in the presence of a tumour. Taken together, these findings could help identify new therapeutic avenues for treatment of patients with CIBP.

Results

A high proportion of deep body CGRP afferents express little or no Advillin

To study bone afferents in the absence of a selective marker, we injected the retrograde tracer fast blue (FB) into the tibial cavity. All lumbar DRG, ipsi- and contralaterally to the injection were dissected, cryosectioned and analysed. We found 18%, 51%, 24% and 7% of all FB+ cells in L2, L3, L4 and L5 DRG respectively (Fig S1A, B), and no FB+ cells on the contralateral side (Not shown), indicating that our tracing was specific. Next, we showed that the traced tibial afferents stained positively for markers of peptidergic nociceptors (e.g. calcitonin gene-related peptide (CGRP) and TrkA, a receptor for NGF), but were rarely positive for isolectin B4 (IB4), a marker for non-peptidergic neurons (Fig S1A, B).

We examined co-expression of a virally delivered genetically-encoded calcium indicator (AAV9-GCaMP6s) and a commonly used marker for sensory neurons, Advillin (Avil). We performed this analysis using a knock out-validated antibody[13]. Surprisingly, around 40% of FB/GCaMP++ cells were Avil negative (Fig. S1C). To ensure validity, we investigated FB-traced tibial afferents from rats that were not subjected to GCaMP6s delivery. The tissue was co-stained for CGRP and TubulinβIII (TubβIII, a known pan-neuronal marker) to further ensure the presence of well-defined neuronal populations (Fig. 1A and S1D). Almost 41% of tibial afferents did not express Avil (Fig. 1B). These Avil negative fibres often (55%) co-localise with CGRP (Fig. 1B). Similarly, in the mouse, we employed a PACT-clearing technique[14] to visualise all neurons within the DRG of Avil-eGFP mice. Counterstaining with CGRP revealed a discrete population of CGRP+, Avil- neurons (around 10% of the total) (Fig.1C, S1E, See also Movie 1, 2). A search through two separate, publicly

bioRxiv preprint doi: https://doi.org/10.1101/498980; this version posted December 17, 2018. The copyright holder for this preprint (which was not certified by peer review) is the author/funder. All rights reserved. No reuse allowed without permission.

available single-cell RNA sequencing databases further supported our finding of differential expression between CGRP (and Tac1, a gene for substance P, another peptide found in peptidergic nociceptors) and Avil in sensory neurons (Fig. S2A, B)[15,16].

Cancer progression impacts bone innervation

We investigated how the presence of bone cancer affects these patterns of innervation by generating a validated rat CIBP model using syngeneic mammary gland carcinoma cells (MRMT1)[17]. We evaluated bone damage caused by cancer growth using a high-resolution micro-computer tomography technique (µCT) at two different time points: days 7/8 and days 14/15. Significant damage to the trabecular bone occurred in both stages, while cortical bone was impaired at days 14/15 only, suggestive of early versus late stage modelling of CIBP (Fig. 2A, see also 3D-visualisation in the Movie 3). Volumetric reconstruction enabled bone mineral density (BMD) quantification for the whole tumour growth area. Reduction of trabecular BMD from around 101-120 mg/cm^3 in sham groups to 45-62 mg/cm^3 in respective CIBP groups, and cortical BMD from 485 mg/cm^3 in the sham late group to 146 mg/cm^3 in the CIBP late group, tightly reflects visually evident bone lesions (One Way ANOVA [group]: trabecular BMD: $F_{3, 18} = 6.272$, $P < 0.0042$, Tukey post-hoc: CIBP early vs. Sham early $P < 0.05$, CIBP late vs. Sham early $P < 0.01$, CIBP late vs. Sham late $P < 0.05$; cortical BMD: $F_{3, 19} = 35.57$, $P < 0.0001$, Tukey post-hoc: CIBP late vs. all the others $P < 0.0001$) (Fig. 2B). Damage to afferents innervating cancerous tissue was quantifiable using activating transcription factor 3 (Atf3), a protein induced by cellular stress[18]. Representative micrographs of the L3 DRG ipsilateral to the injury site clearly demonstrated the characteristic nuclear expression pattern of Atf3 in bone and other afferents (Fig. 2C). This is especially evident in early stages of our CIBP model (Fig. 2F, S2A, B). Interestingly, by the late stage, Atf3 positivity normalises in both groups, with almost no occurrence in late-stage sham animals, suggesting full postsurgical recovery (One Way ANOVA [group]: $F_{3, 17} = 14.37$, $P < 0.0001$, Tukey post-hoc: CIBP early vs. Sham early $P < 0.0001$, CIBP early vs. CIBP late $P < 0.01$, Sham late vs. Sham early $P < 0.01$) (Fig. 2F, S2A, B). Bone afferents are more likely than other afferents to express Atf3 at early disease stages, suggesting higher levels of stress in this population (One Way ANOVA [group]: $F_{3, 17} = 8.844$, $P < 0.001$, Tukey post-hoc: CIBP early vs. all the others $P < 0.01$) (Fig. 2G). Moreover, there is

bioRxiv preprint doi: https://doi.org/10.1101/498980; this version posted December 17, 2018. The copyright holder for this preprint (which was not certified by peer review) is the author/funder. All rights reserved. No reuse allowed without permission.

a visible shift in the expression pattern of Atf3+/FB+ from L3 to L4 DRG between early and late CIBP (Fig. S2B).

To examine whether tumour progression translates to animal behaviour, we monitored rats for up to 16 days after cancer cell implantation. Body weight gain remained stable in this period when compared to the sham animals (Fig. S2C). Behavioural data clearly demonstrate that animals with CIBP manifest mechanical hypersensitivity, with significant changes in static weight bearing between rear legs starting at day 7 post-surgery and progressing with time (CIBP: Kruskal-Wallis for independent samples [days]: $P < 0.0001$: day 2 and day 7 vs. baseline $P < 0.05$, day 14 vs. baseline $P < 0.001$) (Fig. 2H). Sham animals did not demonstrate any significant alterations in the weight-bearing test after day 7, confirming valid model establishment. Sham surgery did affect pain thresholds in the first 2 days suggesting the presence of transient postsurgical pain (Sham: Kruskal-Wallis for independent samples [days]: $P < 0.05$: day 2 vs. baseline $P < 0.01$) (Fig. 2H).

DRG afferents encode mechanical pressure stimuli in a graded fashion

We implemented *in vivo* GCaMP6s imaging to thoroughly analyse bone afferent physiology in the late cancer stage since mechanical hypersensitivity was evident most clearly here. Considering our anatomical findings of low Avil expression in bone afferents, we opted for intrathecal delivery of an AAV9 viral vector containing GCaMP6s. This method of delivery was previously shown by our lab to ensure uniformly distributed expression between all subtypes of the DRG neurons[19] and Fig. S1). We analysed 757 DRG neuronal cell bodies from 9 sham-operated rats, and 1750 neurons from 10 CIBP animals transduced with AAV9/Syn.GCaMP6s. Lumbar DRG L3 and L4 were imaged (based on our FB tracing studies (Fig. S1, Fig. 2D, E, and[18,20]), and 6-7 L3 DRG and 3 L4 DRG from each group were imaged. No response difference was detected between L3 and L4 lumbar levels (not shown), hence results from all DRG were pooled.

To apply pressure stimuli, we implemented a novel method using a neonatal cuff connected to a manometer and air pump. The cuff was applied sequentially in all animals to the following rear limb regions: knee and tibial head, calf, and calf-ankle. Incremental pressure (50 mmHg every 10 s, in the range of 0-400 mmHg) was applied (Fig. 3A, S3A). Utilising this stimulation regimen, individual DRG neurones showed phasic and tonic increases in Ca^{2+} when pressures were increased (Fig.

bioRxiv preprint doi: https://doi.org/10.1101/498980; this version posted December 17, 2018. The copyright holder for this preprint (which was not certified by peer review) is the author/funder. All rights reserved. No reuse allowed without permission.

3B). In addition to cuff stimulation, we also examined proprioceptive responses, by gently moving the limb along the body axis in 5 consecutive push-pull stretching cycles. Our results were analysed using in-house R scripts. Very stringent criteria were applied in order to select responses: fluorescence intensity was counted as a positive response when an average signal reached 70% above baseline fluorescence plus 4 standard deviations[19].

A striking difference in the number of neurons recruited between sham and CIBP groups, especially after the knee compression (which mostly covered the tumour-growth area) was clear. The effect was detected with the naked eye on video-rate recording (Movie 4). Selected frames from before and after stimulation (Fig. 3C) further illustrate the large magnitude of our effect. An almost 3-fold increase in the total number of responding cells, from around 6% in sham to 18% in CIBP after knee compression (RM-ANOVA [group]: $F_{1, 2505} = 50.233$, $P < 0.0001$) (Fig. 3D), and an around 2-fold increase for gentle leg movement without mass bearing (RM-ANOVA [group]: $F_{1, 1335} = 31.338$, $P < 0.0001$) (Fig. 3E, S3B) was observed. Interestingly, increased compression forces (range 100-400 mmHg) were reflected in the linear recruitment of responders in the CIBP group (Fig. 3D). In contrast, the number of responders in sham group did not appear to increase linearly. There appeared to be a threshold between 50-100 mmHg, after which all potential mechanoceptors within the imaged field of view (FOV) were responding to the chosen receptive field stimulation (Fig. 3D).

Contrary to cell number, the fluorescent intensity of responders was not altered in the CIBP rat model between sham and cancer groups, neither after knee compression, nor leg movement (RM-ANOVA [group]: knee compression: $F_{1, 489} = 0.312$, $P = 0.577$; leg movement: $F_{1, 566} = 0.107$, $P = 0.744$) (Fig. 4A, B, S4A, B). Fluorescent intensity coded in line with the pressure surge applied to the knee in both groups (Fig. 4A). Unlike cuff pressure, proprioception appears to be encoded by the same cells responding to different leg positions (push-pull stretches) without the change in fluorescence (Fig. 4B, S4B).

CIBP recruits previously silent nociceptive C fibres

We analysed the cell size distribution of responders in healthy and cancer states. We chose 700 μm^2 and 1200 μm^2 to crudely separate sensory neuron type (small and medium-size cells). Our results suggest that pressure is encoded mainly

bioRxiv preprint doi: https://doi.org/10.1101/498980; this version posted December 17, 2018. The copyright holder for this preprint (which was not certified by peer review) is the author/funder. All rights reserved. No reuse allowed without permission.

by small to medium-size neurons. As expected, the average cell size decreased with the increase of the force applied (Fig. 4C). Intriguingly, there were significant differences in the average cell sizes of responders to knee compression (RM-ANOVA [group]: $F_{1, 202} = 16.24$, $P < 0.0001$) (Fig. 4C), but not leg movement (RM-ANOVA [group]: $F_{1, 303} = 0.239$, $P = 0.625$) (Fig. 4D, S4C), between cancer and sham animals. Specifically, in sham animals, the number of medium-size responders increased with increasing stimulus pressure (Fig. 4E), while dynamic brushing of the calf only recruited a few large-sized neurons. Meanwhile, in our cancer group, an additional population of small diameter neurons (likely C nociceptors) was activated proportionally with increasing stimulus strength, reaching almost 3 times the number of cells that responded to the 400 mmHg than the initial 50 mmHg (Fig. 4E).

Intratibial afferent function in health and CIBP

We next focused on bone afferents using FB tracing. Firstly, we investigated whether the neurons innervating the tibial cavity express Piezo-type mechanosensitive ion channel component 2 (Piezo2) and TrkA; an abundance of both proteins on bone afferents was observed (Fig. 5A). Secondly, we examined the functional responses of bone afferents (Fig. 5B, C, D). Sensory cells innervating tibial cavity were responsive to whole limb mechanical stimulation (Fig. 5E, S5A). Around 13% of traced tibial cavity afferents responded to knee compression (Fig. 5E), and considerably more responders (~25%) were observed following calf compression (Fig. S5A). Leg movement activated up to 25% of all traced cells (Fig. 5F). Compared to non-traced cells (Fig. 3D), the engagement of FB+ responders to their receptive field compression required higher pressures (around 200 mmHg) (Fig. 5E), suggesting that bone has a higher pressure activation threshold than more cutaneous layers.

Interestingly, there was no difference between sham and cancer-bearing groups regarding the number of responders to knee compression and movement (RM-ANOVA [group]: knee compression: $F_{1, 313} = 0.286$, $P = 0.593$; leg movement: $F_{1, 209} = 0.037$, $P = 0.848$) (Fig. 5E, F). Fluorescence intensity of bone afferents after knee compression was equally unaffected by the presence of cancer (RM-ANOVA [group]: $F_{1, 50} = 0.577$, $P = 0.451$) (Fig. 5G). In contrast, leg movement resulted in almost two times lower fluorescence in CIBP compared with sham animals (RM-ANOVA [group]: $F_{1, 82} = 8.507$, $P < 0.01$) (Fig. 5H).

bioRxiv preprint doi: https://doi.org/10.1101/498980; this version posted December 17, 2018. The copyright holder for this preprint (which was not certified by peer review) is the author/funder. All rights reserved. No reuse allowed without permission.

Muscle and periosteum afferents are recruited and sensitized by bone cancer

Bone afferents were not sensitised in CIBP but what about local periosteum and muscle afferents? Analogous to the bone afferents we traced muscle and periosteum (MP) afferents by injecting AAV-retrograde virus expressing tdTomato outside the tibia (Fig. 6A, B, C). Piezo2 and TrkA were both present in the traced cells (Fig. 6D). Further, we showed that virtually none of the MP traced cells from the sham group responded to mechanical stimulation (Fig. 6E, S6A, B). However in the cancer state 20% of traced MP afferents responded to the knee compression, and around 36% responded to the leg movement (RM-ANOVA [group]: $F_{1, 52} = 3.077$, $P = 0.085$) Fig. 6E, S6A, B). Similarly, to total DRG cell analysis (Fig. 3D), the number of responders increased with compression intensity. The responders' fluorescence intensity increased linearly with the stimulus strength but plateaud at around 300 mmHg (Fig. 6F, S6A).

Pharmacological block of Piezo2 inhibits activated silent nociceptors

NGF-mediated sensitization is thought to occur via Piezo2 channels[21]. We observed the 'un-silencing' of dormant nociceptors in CIBP. Hence, we blocked Piezo2 locally by injecting the muscles surrounding the cancer-bearing bone with tarantula *Grammostola spatulate* toxin (GsMTx4) (Fig. 7A). This venom peptide potently inhibits cationic mechanosensitive channels, including Trpc1, Trpc6 and Piezo2[22,23]. Previously, GsMTx4 effectively blocked Piezo2 currents *in vitro*, resulting in the 're-silencing' of silent nociceptors previously unmasked by NGF[21]. Here, we show that the toxin has a similar effect *in vivo*: GsMTx4 (10 µg in 50 µl saline) delivered to cancer rats significantly reduced the number of responding cells to knee compression after 40 minutes (RM-ANOVA [time]: $F_{2, 1689} = 6.704$, $P < 0.001$, Bonferroni post hoc: 40 min. vs. Baseline $P < 0.007$, 40 min. vs. 20 min. $P < 0.003$), practically returning the percentage of responders back to sham-operated levels (Fig. 7B, C). No change in response to GsMTx4 injection was observed i sham animals following knee compression (not shown). Fluorescence intensity of responders was not significantly altered in the cancer group (RM-ANOVA [time]: $F_{2, 447} = 1.739$, $P = 0.177$) (Fig. 7D).

bioRxiv preprint doi: https://doi.org/10.1101/498980; this version posted December 17, 2018. The copyright holder for this preprint (which was not certified by peer review) is the author/funder. All rights reserved. No reuse allowed without permission.

Discussion

Malignant tumours can escape their origin and invade distant regions of the body to form secondary tumours. A frequent direction for metastasis is the skeleton. In this study, we identified a discrete population of peripheral neurons that innervate bone and lack Avil expression. Using *in vivo* calcium imaging, we also revealed novel mechanisms that drive cancer-induced bone pain.

A high proportion of deep body CGRP afferents express little to no Advillin

We demonstrate that many bone afferents express markers of peptidergic (e.g. CGRP and TrkA), but rarely non-peptidergic (IB4) nociceptors, in agreement with previous reports[9,24–26]. Further, we discovered that a large population of bone afferents rich in CGRP lack Avil expression. Over the last decade there have been repeated efforts to more accurately define sub-populations of sensory neurones[15]. Avil, an actin-binding protein, was anticipated to be selectively expressed by up to 97% of all sensory DRG cells[27]. Following this announcement, several murine models were created to drive transgene expression utilising *Avil*. Recent research suggests that Avil is expressed not only in sensory neurons, but in most adult neural crest-derived neurons including sympathetic fibres[13]. Others reported that Avil-driven transgene expression does not cover around 10-15% of sensory neurons. A restriction to any particular population of the DRG cells, however, was not described[28,29]. Publicly available single-cell RNA sequencing databases supported our finding of differential expression between CGRP and Avil on the whole population level[15,16]. Overall the presence of a discrete (around 10% of all DRG neurons) but significant population of peptidergic afferents that are low or almost not expressing Avil, although enriched in CGRP, is reported. This type of afferent appears to be particularly abundant in bone innervation. The physiological meaning of the lack of Avil in bone afferents remains an open question, not least since the exact function of Avil is unknown.

Cancer progression impacts bone innervation

We employed a highly-validated rat CIBP model[17] and analysed bone afferent response to the tumour. Firstly, based on the high-resolution micro-computer tomography results and individual animals ability to weight bear, we divided the model into early and late stages of bone cancer: days 7/8, defined by damage of trabecular but not cortical bone, and imbalance in weight bearing <10%; versus days

bioRxiv preprint doi: https://doi.org/10.1101/498980; this version posted December 17, 2018. The copyright holder for this preprint (which was not certified by peer review) is the author/funder. All rights reserved. No reuse allowed without permission.

14/15, defined by damage of both trabecular and cortical bone, and imbalance in weight bearing >10%. Secondly, we showed that afferents innervating cancer-bearing bones are sensitized in the early stage with high expression of cellular stress marker Atf3. In the late cancer stage, the activation of Atf3 appears resolved. Multiple mechanisms may contribute to the reduction of Atf3 in the late stages of cancer. It is possible that CIBP afferents are undergoing cell death as a result of tumour invasion and toxic local conditions. Supporting this hypothesis is an observed shift in the expression pattern of Atf3+/FB+ from L3 to L4 DRG between early and late CIBP, further indicating the presence of a degenerative mechanism in L3 tibial afferents, and consecutive sprouting and/or activation of L4 afferents.

The reluctance of CIBP rats to bear weight on the cancer-loaded leg corresponds to the clinic, where CIBP often manifests as a result of musculoskeletal compression, both due to weight bearing in moving subjects and increased intraosseous pressure secondary to tumour expansion[30,31,17,32]. Indeed, mechanical pain is the most commonly reported type of pain in bone cancer patients[3]. Given the above evidence, we studied mechanosensation in the CIBP rats using *in vivo* imaging with GCaMP6s.

DRG afferents encode mechanical pressure stimuli in a graded fashion

Pressure and mechanosensation coding is investigated on both a molecular[33,34] and neuronal system levels[35,36]. How is modality-reflecting information encoded by sensory neurons? We took the opportunity to analyse DRG cells that responded to mechanical simulation, observing closely whether these cells encoded the analysed stimuli.

The analysed DRG neurons responded globally to pressure in line with the compression force increase. Graded coding of compression, which is maintained in both health and disease, is thus likely. In contrast, gentle leg movement likely activating proprioceptors appears encoded by the same cells responding to different leg positions without the change in the fluorescence. This most likely reflects combinatorial coding, where different firing patterns of a cell encode changes in leg position. Whether the information is encoded in different temporal forms of impulses needs to be verified utilising methodologies offering higher temporal resolution (i.e. electrophysiology). Similar coding strategies appear to be true for bone afferents, in

bioRxiv preprint doi: https://doi.org/10.1101/498980; this version posted December 17, 2018. The copyright holder for this preprint (which was not certified by peer review) is the author/funder. All rights reserved. No reuse allowed without permission.

agreement with previously reported electrophysiological studies researching tibial axons and increased intraosseous pressure[30,31].

CIBP recruits previously silent nociceptive C fibres

We showed that pressure is encoded mainly by small to medium-size neurons. As expected, the average cell size decreased as the force applied increased (increasingly painful levels of pressure recruit small nociceptive afferents preferentially over large myelinated Aβ mechanosensors). Previously, dynamic brushing on the calf surface proved that light touch is encoded by Aβ fibres[19,37].

We found a three-fold increase in the number of neurons responding to knee compression in CIBP, as compared to sham animals. Interestingly, these cells were small to medium-size, in contrast to results obtained from sham animals where pressure activated mainly medium-size neurons. The latter is in keeping with previous literature which suggests that in healthy animals, noxious compression is encoded preferentially by myelinated Aδ nociceptors[30]. The robust recruitment of cells, in particular a large cluster of small-size cells, in CIBP rats suggests activation of previously silent nociceptors. The existence of these kinds of fibres has been reported before[38], but never in the context of cancer.

Next, we went on to investigate where these silent nociceptors might originate from. We traced afferents from within the bone with FB and found that they respond to mechanical forces, as demonstrated previously by electrophysiology[30,31]. However, no additional recruitment was detected in this neuronal population suggesting that silent nociceptors in late cancer stage originate outside of the bone. Again, we observed linear coding of pressure, in agreement with previous electrophysiological reports of tibial axon coding to increasing intraosseous pressure [30,31]. The reduced fluorescence of bone afferents to the proprioceptive stimulation in CIBP animals suggests impaired bone proprioceptor functioning and/or their loss in tumour conditions.

These functional results support our anatomical findings (decreased Atf3 staining in the late CIBP group) (Fig. 2G, S2) and suggesting a degree of bone afferent loss in advanced cancer states. This is also supported by the shift in FB positivity that occurs from L3 to L4 DRG in the late stage CIBP (Fig. S2). The anaerobic and toxic conditions of the tumour are likely to evoke degeneration of locally entrapped afferents.

bioRxiv preprint doi: https://doi.org/10.1101/498980; this version posted December 17, 2018. The copyright holder for this preprint (which was not certified by peer review) is the author/funder. All rights reserved. No reuse allowed without permission.

Silent nociceptors in CIBP originate from muscle or periosteum via a Piezo2-dependent mechanism

Since bone afferents themselves do not appear to be the neurons responsible for sensitization, we next used a viral approach to label MP afferents. We found them to be silent in sham operated animals, but responsive in cancer conditions. This suggests that in the late stage of the disease, cancer induces employment of silent nociceptors from bone surroundings, rather than the bone cavity itself. Our anatomical results must be taken with some care. Virally-delivered tdTomato expression levels around the bone remained low and we had to limit the amount of virus used to ensure specificity and to avoid off-target labelling in contralateral DRG. This meant that our cell numbers were low compared to the rest of our analyses (Fig. 6B, C).

Finally, a recent study suggested that silent nociceptors are 'un-masked' by NGF via TrkA and Piezo2[21]. As CIBP is well-known to be NGF-dependent[5,39], these typically quiescent MP afferents could significantly contribute to the development of this pain phenotype. Indeed, here we found evidence that recruitment of silent afferents in CIBP is Piezo2 dependent. Retrogradely traced MP afferents express Piezo2 and blockade of Piezo2 activity using the tarantula toxin (GsMTx4) resulted in a potent reversal of the number of compression-responsive cells. The effect appeared specific, since baseline responsiveness of remaining mechanoceptors to mechanical stimuli was unaffected.

Conclusions

In agreement with Prato and colleagues[21], we provide evidence that silent nociceptors are present in deep tissues. In our model of CIBP they are activated to potently increase nociceptive input to the CNS. We hypothesise that locally released NGF unlocks these dormant cells leading to additional nociceptive signalling in the spinal cord, ultimately amplifying pain perception (Fig. 7E). This mechanism may be one of the reasons why bone cancer patients experience a unique type of mechanoceptive pain even after remission: silent nociceptors may remain active. Anti-NGF therapy could therefore benefit this patient population in two ways. First, by limiting sprouting of afferents into the affected bone and second, by preventing recruitment of silent nociceptors from the surrounding muscle.

bioRxiv preprint doi: https://doi.org/10.1101/498980; this version posted December 17, 2018. The copyright holder for this preprint (which was not certified by peer review) is the author/funder. All rights reserved. No reuse allowed without permission.

Finally, we hypothesise that Piezo2 plays a critical role in unsilencing nociceptors in cancer. The channel, with its variety of splice variants, has been established as a definitive mechanosensitive protein in mammalian tissue[33]. We are yet to confirm which isoform is the most important in the mechanism described here, but our data suggests that Piezo2 blockers could be a valuable additional target in the fight against CIBP.

Materials and Methods

Cell lines

Syngeneic rat mammary gland adenocarcinoma cells (MRMT-1, Riken cell bank, Tsukuba, Japan) isolated from female Sprague-Dawley rat, were cultured in RPMI-1640 medium (Invitrogen, Paisley, UK) supplemented with 10% FBS, 1% L-glutamine and 2% penicillin/streptomycin (Invitrogen, Paisley, UK). All cells were incubated at 5% CO_2 in a humidity-controlled environment (37 °C, 5% CO_2; Forma Scientific).

Animals

Male Sprague-Dawley rats (UCL Biological Services, London, UK or Charles-River, UK), C57/BL6 mice (Charles-River, UK), and Avil-GFP mice [see gensat.org: STOCK Tg (Avil-EGFP) QD84Gsat/Mmucd for BAC expression levels] were used for experiments. Avil-GFP mice were bred in-house for several generations onto a C57/BL6J background. In all experiments, adult, age-matched (3–6 month) littermate controls from both genders were used. Animals were group housed on a 12:12-hour light–dark cycle. Food and water were available *ad libitum*. Animal house conditions were strictly controlled, maintaining stable levels of humidity (40-50%) and temperature (22±2°C). All procedures described were approved by the Home Office and adhered to the Animals (Scientific Procedures) Act 1986. Every effort was made to reduce animal suffering and the number of animals used in accordance with IASP ethical guidelines[40].

Cancer-induced bone pain model

On the day of surgery, MRMT-1 cells were released by brief exposure to 0.1% w/v trypsin-ethylenediaminetetraacetic acid (EDTA) and collected by centrifugation in medium for 5 min at 1000 rpm. The pellet was washed with Hanks' balanced salt

bioRxiv preprint doi: https://doi.org/10.1101/498980; this version posted December 17, 2018. The copyright holder for this preprint (which was not certified by peer review) is the author/funder. All rights reserved. No reuse allowed without permission.

solution (HBSS) without calcium, magnesium or phenol red (Invitrogen, Paisley, UK) and centrifuged for 5 min at 1000 rpm. MRMT1 cells were suspended in HBSS to a final concentration of 300,000 cells/ml and kept on ice until use. Only live cells were counted with the aid of Trypan Blue (Sigma) staining. Cell viability after incubation on ice was checked after surgery, and no more that 5-10% of cells were found dead after 4 h of ice-storage.

Sprague-Dawley rats weighting 120-140 g (for late-stage CIBP, 14 days post-surgery) or 180-200 g (for early-stage CIBP, 7 days post-surgery), following complete induction of anaesthesia with isoflurane (induction 5%, maintenance 1.5-2%) in 2 l/min O_2 and subcutaneous perioperative meloxicam injection (50 µl 2 mg/kg, Metacam®, Boehringer Ingelheim, Berkshire, UK), were subjected to the surgical procedure of cancer cell implantation into the right tibiae [17]. Briefly, in aseptic conditions, a small incision was made on a shaved and disinfected area of the tibia's anterior-medial surface. The tibia was carefully exposed with minimal damage to the surrounding tissue. Using a 0.7 mm dental drill, a hole was made in the bone through which a thin polyethylene tube (I.D. 0.28 mm, O.D. 0.61 mm; Intramedic, Becton Dickinson and Co., Sparks, MD, USA) was inserted 1-1.5 cm into the intramedually cavity. Using a Hamilton syringe, either 3×10^3 MRMT-1 carcinoma cells in 10 µl HBSS or 10 µl HBSS alone (Sham) was injected into the cavity. The tubing was removed, and the hole plugged with bone restorative material (IRM, Dentsply, Surrey, UK). The wound was irrigated with saline and closed with Vicryl 4-0 absorbable sutures and wound glue (VetaBond 3M, UK). The animals were placed in a thermoregulated recovery box until fully awake.

Administration of tracers and calcium indicators

Male Sprague-Dawley rats weighting 60-70 g, following complete induction of anaesthesia with isoflurane (induction 5%, maintenance 1.5-2%) in O_2 (2 l/min) were maintained at around 37°C using a homeothermic heating mat and 50 µl of Meloxicam (2 mg/kg, Metacam®, Boehringer Ingelheim, Berkshire, UK) was subcutaneously administered for post-operative pain management. Animals were fixed in a stereotaxic apparatus (Kopf, Germany), their lumbar region was clamped and spinal T12-L1 intervertebral space was exposed by bending the lumbar region rostrally providing easy access to the underlaying dura without the need for laminectomy. A small puncture in the dura was made and a thin catheter of 0.2 mm

bioRxiv preprint doi: https://doi.org/10.1101/498980; this version posted December 17, 2018. The copyright holder for this preprint (which was not certified by peer review) is the author/funder. All rights reserved. No reuse allowed without permission.

diameter (Braintree Scientific) was inserted in the caudal direction. 10 µl of AAV9.CAG.GCaMP6s.WPRE.SV40 was infused into the intrathecal space at 1.2 µl/min (titer ≥ 1×10^{13} vg/ml, cat. 100844-AAV9, Addgene, US). Due to the length of the inserted cannula, the infusion was close to L4 DRG. The catheter was left in place for 2 minutes before slow withdrawal. The incision was closed with wound clamps and postsurgical glue (Vetabond, 3M, UK). After 7 days of recovery, left tibia was injected with 5 µl of 4% Fast Blue neuronal tracer (Polysciences Inc., Germany) as described above, allowing tracing of bone afferents. The muscle layer adjacent to Fast Blue injected bone was injected at the same time with 5 µl of pAAV-CAG-tdTomato (titer $7x10^{12}$ vg/ml, 59462-AAVrg, Addgene, US) to allow tracing of muscle and periosteum afferents. After a 7-day recovery period, animals were randomly divided into two groups receiving either cancer cells or sham HBSS buffer treatment into the left tibia (injection was through the same hole in the bone to prevent further damage). Two weeks after cancer implantation animals were subjected to terminal *in vivo* calcium imaging. Throughout the whole period, body mass was carefully monitored, and animals steadily gained weight resulting in 250-280 g at the day of imaging.

In vivo calcium imaging of sensory neurons

Rats were anaesthetised using urethane (12.5% w/v in saline, Sigma, UK). Starting with an initial dose of 0.5 ml given i.p., subsequent (0.5ml) given at approximately 10-15 minute intervals, depending on hind limb reflex activity, until surgical depth was achieved. The core body temperature was maintained close to 37°C using a homeothermic heating mat with a rectal probe (Harvard Apparatus). Tracheotomy was performed to secure steady breathing. An incision was made to the skin on the back and the muscle overlying the L3, L4 and L5 vertebral segment was removed. The bone around either the L3 or L4 DRG was carefully removed and the underlying epineurium and dura mater over the DRG were washed and moistened with normal saline. The position of the animal's body was varied between prone and lateral recumbent to orient the DRG in a more horizontal plane. The exposure was then stabilised at the neighbouring vertebrae using spinal clamps (Precision Systems and Instrumentation) attached to a custom-made imaging stage. The exposed cord and DRG were covered with silicone elastomer (World Precision Instruments, Ltd) to avoid drying and to maintain a physiological environment. The

bioRxiv preprint doi: https://doi.org/10.1101/498980; this version posted December 17, 2018. The copyright holder for this preprint (which was not certified by peer review) is the author/funder. All rights reserved. No reuse allowed without permission.

rat was then placed under the Eclipse Ni-E FN upright confocal/multiphoton microscope (Nikon) and the microscope stage was variably diagonally orientated to optimise focus on the DRG. The ambient temperature during imaging was kept at 32°C throughout. All images were acquired using a 10X dry objective. To obtain confocal images a 488 nm Argon ion laser line was used. GCaMP signal was collected at 500-550 nm. Time series recordings were taken with an in-plane resolution of 512 x 512 pixels and a fully open pinhole for video-rate acquisition.
Image acquisition varied between 2-4 Hz depending on the experimental requirements and signal strength. At the end of the experiment, rats were sacrificed by clamping the trachea tube and left for 1h for the DRG to fill up with calcium for maximum signal control.

Activation of sensory neurons for GCaMP *in vivo* imaging

Throughout the experiment, care was taken to provide sufficient breaks between stimuli (usually 3-5 min) in order for the tissue to equilibrate back to its baseline state. Mechanical stimulation consisted of brushing the ipsilateral calf, stretching the leg and pressure application to the leg. Brushing was performed for 10 s to the shaven surface of the cancer-bearing calf. The leg was stretched by a cycle of 10 x gentle pulling and pushing of the ipsilateral leg rostro-caudally along the body axis. Finally, incremental pressure (50 mmHg increments every 10 s, in the range of 0-400 mmHg) was applied to the leg using a neonatal cuff connected to a manometer and air pump (air-filled 20 ml syringe). The cuff was consecutively positioned in 3 places: knee-tibial head, calf, and calf-ankle.

Pharmacological block of Piezo2

In a subset of experiments (CIBP – 3 animals and Sham – 2 animals) after stable responses to the standard baseline activation of sensory neurons, rats were injected in the muscle tissue surrounding cancer-bearing tibia on each side of the bone with 2 x 25 µl (5 µg each side in saline) of GsMTx4 toxin (Tocris, UK). Following injections, two recordings, 20 and 40 min post injection, to knee pressure cuff stimulation were collected. A vehicle (saline) injection was performed before each drug application.

Calcium imaging data analysis

Drift in time-lapse recordings was corrected using NIS Elements AR 4.30.01 (Nikon, align application). Further image processing was done using Fiji/ImageJ Version

bioRxiv preprint doi: https://doi.org/10.1101/498980; this version posted December 17, 2018. The copyright holder for this preprint (which was not certified by peer review) is the author/funder. All rights reserved. No reuse allowed without permission.

1.52h, and graphing and statistical analysis was undertaken with a combination of Microsoft Office Excel 2013, IBM SPSS Statistics 25 package and RStudio 0.99.893. In order to generate traces of calcium signals from time lapse images, regions of interest (ROIs) surrounding cell bodies were chosen using a free hand selection tool in Fiji. ROIs were chosen with minimal overlap to ensure less interference from surrounding somata. A region of background was selected, and its signal subtracted from each ROI. To generate normalised data, a baseline period of fluorescence was recorded for each ROI and changes from this baseline fluorescence were calculated as ΔF/F and expressed in percentages [19]. Implemented here are stringent criteria, where an average signal reaching 70% above baseline fluorescence plus 4 standard deviations were qualified as a response. Percentage of responders was quantified in a binary fashion within all selected ROIs. The fluorescence intensity and size analysis was performed only for responders. Non-responding cells were not analysed for their fluorescence intensity levels, as it would artificially introduce biased zero values for these cells which were either non-responding for the particular modality, or were outside of the stimulated receptive field. Thus, only those cells were analysed for intensity and size, which responded at least once to the given stimulus modality (i.e. knee compression 0-400 mmHg).

Static Weight Bearing

Behaviour was assessed 2-4 hours before surgery (day 0) and at 2, 7 and 14 days following cancer cell injection. Testing was preceded by a 30 min acclimatisation period. Rooms conditions used for behavioural testing were strictly controlled, maintaining stable levels of humidity (40-50%) and temperature (22±2°C). Weight bearing was assessed using a tester (Linton Instrumentation, Norfolk, UK) in which rats were placed in a plexiglass enclosure where each hindpaw rested on a separate weighing plate. After a few minutes of habituation, the force exerted by each hind paw was measured 5 times with a 10-20 s gap between measurements. Measurements from each paw separately were averaged, and results were transformed to give the percentage of weight borne on each side to the total rear legs bearing (taken as 100%).

Micro-computed tomography of cancer-bearing legs

Rats were sacrificed by overdose of isoflurane (5% vol/vol) and transcardially perfused with 250 ml of cold phosphate buffer saline solution (PBS, pH=7.5,

bioRxiv preprint doi: https://doi.org/10.1101/498980; this version posted December 17, 2018. The copyright holder for this preprint (which was not certified by peer review) is the author/funder. All rights reserved. No reuse allowed without permission.

Invitrogen, Paisley, UK) followed by 4% paraformaldehyde solution in 0.1 M phosphate buffer (250 mL, pH=7.5, Sigma, UK). Bones were stored frozen in -20°C until analysis. Rat tibiae, cleared of excess muscle and soft tissue, were placed into a micro-computed tomography scanner (µCT, Skyscan1172) with Hamamatsu 10 Mp camera. Recording parameters were set as follows: source voltage at 40 kV, source current at 250 µA, rotation step at 0.600 deg, with 2 frames averaging and 0.5 mm aluminium filter. For reconstruction NRecon software (version: 1.6.10.4) was used. In total, over 500, 34 µm thick virtual slices were collected per bone. Because the reference point for rat's tibia for micro-CT analysis was not previously described, we established an anatomically relevant reference point which was not affected by cancer, from which a region of interest was chosen for further analysis. Reference point for bone mineral density analysis (BMD) was defined as the internal tip of the intercondylar area, which was consistently located at 5 mm from the centre of the cancer growth zone. For BMD, the cancer growth zone encompassing space between 3 to 7 mm caudally from the reference point was quantified. A total of 119 scanned planes, each with a thickness of 34 µm, was analysed (see figure S3A for more details). Comparison to two known density standards allowed us to quantify BMD values in mg/cm^3 of both trabecular and cortical bone (utilising dataViewer software). Representative visualisations were prepared with Fiji with 3D viewer plugin.

Immunohistochemistry

For experiments which did not involve *in vivo* imaging, animals were sacrificed by overdose of pentobarbital (Euthanal, Merial, UK) and transcardially perfused with 250 ml of cold phosphate buffer saline solution (PBS, pH=7.5, Invitrogen, Paisley, UK) followed by 4% paraformaldehyde solution in 0.1 M phosphate buffer (250 mL, pH=7.5, Sigma, UK). The lumbar 1-6 dorsal root ganglia (DRG) from both injured (ipsilateral) and intact (contralateral) sides were collected and post-fixed overnight in 4% paraformaldehyde (PFA) at 4°C followed by cryoprotection in 30% sucrose (with 0.02% sodium azide) for 24 hours.

Alternatively, at the end of each GCaMP imaging experiment L1-L5 ipsi/contra DRG were collected and post-fixed overnight in 4% paraformaldehyde (PFA) at 4°C followed by cryoprotection in 30% sucrose (with 0.02% sodium azide) for 24 hours. After cryoprotection all DRG were embedded in Optimal Cutting Temperature

bioRxiv preprint doi: https://doi.org/10.1101/498980; this version posted December 17, 2018. The copyright holder for this preprint (which was not certified by peer review) is the author/funder. All rights reserved. No reuse allowed without permission.

(Tissue-Tek) and stored at -80°C for further analysis. The DRG embedded in OTC mould were cryo-sectioned (Bright Instruments, UK) to 10 µm thick slices collected on Menzel-Gläser Superfrost Plus Slides (25x75x1.0 mm) and stored in -20°C freezer until staining. Once dried (45°C for 2 hours) and briefly washed with 50% ethanol, sections were outlined with a hydrophobic marker (PAP pen, Japan), rehydrated and blocked with 10% donkey serum in washing solution (0.01% NaN_3, 0.3% Triton X-100 in PBS, pH=7.5) for two hours prior to overnight incubation at room temperature with primary antibodies against Atf3 (rabbit, 1:200, Santa Cruz, (C-19): sc-188, US), TubβIII (mouse, 1:1000, G712A, Promega, UK), GFP (to visualise GCaMP6s; chicken, 1:1000, ab13970, Abcam, UK), TrkA (NGF receptor; 1:400, Abcam, ab8871, UK), Piezo2 (Rabbit; 1:200, NBP1-78624SS, NovusBio, UK), CGRP (marker of small peptidergic neurons; 1:500, CA1134, Enzo Life Sciences, UK), CGRP (marker of small peptidergic neurons; 1:1000, ab81887, Abcam, UK), IB4 (conjugated to Alexa Fluor 647; marker of small, non-peptidergic fibres; 1:250, I32450, Molecular Probes, UK), Advillin (Rabbit, 1:500, Abcam, ab72210, UK). Slides were then incubated with the appropriate fluorophore-conjugated secondary antibodies (Goat anti-Chicken, Alexa Fluor 488, A11039, Invitrogen, Eugene, OR, US; Goat anti-Rabbit, Alexa Fluor 594, A11037, Invitrogen, Eugene, OR, US; Goat anti-Rabbit, Alexa Fluor 568, A10042, Invitrogen, Eugene, OR, US; Goat anti-Mouse, AlexaFluor 647, A31571, Invitrogen, Eugene, OR, US; Goat anti-Rabbit, AlexaFluor 647, A21244, Invitrogen, Eugene, OR, US; all used at 1:1000 dilution) for 2 hours at room temperature. Slides were coverslipped using media (Fluoromount-G without DAPI, eBioscience, UK) and stored in darkness at 4°C until imaging.

Samples were typically imaged with an LSM 710 laser-scanning confocal microscope (Zeiss) using 10x (0.3 NA) and 20 x (0.8 NA) dry objectives and analysed with Fiji Win 64. For quantification, samples were imaged with 20x dry objective on Zeiss Imager Z1 microscope coupled with AxioCam MRm CCD camera. The acquisition of images was made in multidimensional mode and the MosaiX function was used to construct the full view. 3-6 DRG were imaged per lumbar region. Cell counting was carried out on the Fiji Win 64 utilising cell counter plugin. For Atf3 analysis, cells were counted as positive only when the cell's nucleus was stained red. The percentage of Atf3 positive cells relative to the total number of neurons (TubβIII) and FB positivity was calculated. On average, 20-30 DRG sections were imaged for quantification.

bioRxiv preprint doi: https://doi.org/10.1101/498980; this version posted December 17, 2018. The copyright holder for this preprint (which was not certified by peer review) is the author/funder. All rights reserved. No reuse allowed without permission.

PACT

A passive CLARITY tissue clearing technique (PACT) (described in detailed in: [14]) has been implemented to allow whole-mount DRG imaging from Avil^{eGFP} mice with minor modifications. Briefly, Avil-GFP mice were deeply anesthetized with pentobarbital and transcardially perfused with cold PBS followed by a cold 4% PFA solution in phosphate buffer, pH=7.5. Lumbar DRG were extracted and post-fixed in 4% PFA overnight in 4°C. After fixation, samples were transferred directly to ice-cold A4P0 solution consisting of: 4% acrylamide monomer (40% acrylamide solution, cat. 161-0140, Bio-Rad, UK), 0.25% VA-044 (thermoinitiator, Wako, US) in 0.01 M PBS, pH=7.4, and incubated at 4°C overnight in prewashed distilled water (to remove anticoagulant) in dried vacutainer tubes (Vacutainer, cat 454087, Greiner GmbH, Austria). The next day, samples were degassed by piercing the septum with a 20G needle connected to a custom-build vacuum line. The residual oxygen was replaced with nitrogen by 5 min bubbling of the solution with pure nitrogen (BOC, UK) via a long, bottom-reaching 20G needle, and a second short needle pierced to allow gases to exhaust. Throughout, samples were kept on ice to prevent heating and consequent premature A4P0 polymerisation. After achieving oxygen-free conditions, samples were polymerised by 3 h incubation in a 37°C water bath. Following polymerisation, the excess honey-like polyacrylamide gel was removed with tissue paper, and samples were transferred to 15-50 ml falcon tubes filled with clearing solution. 10% SDS (cat. L3771, Sigma-Aldrich, UK) in PBS, pH=8.0, was used for passive clearing. Samples were incubated on a rotary shaker at 37°C and 70 rpm (Phoenix Instruments, UK) until reaching the appropriate transparency (usually overnight).

Next, all samples were washed with PBS pH=7.5 on rotary shaker at room temperature, by replacing the solution 4-5 times throughout the course of 1 day in order to remove the SDS. Following washing, samples were treated with primary antibodies in 2% normal donkey serum in 0.1% Triton X-100 in PBS, pH=7.5 with 0.01% sodium azide. The following primary antibodies were used: anti-eGFP (chicken, 1:400, ab13970, Abcam, UK) and anti-CGRP (marker of small peptidergic neurons; 1:200, ab81887, Abcam, UK). 250 µl antibody solution was used per DRG in a 2 ml Eppendorf tube. Samples were incubated with primary antibodies at room temperature, with gentle shaking for 3 days. This was followed by 4-5 washing steps

bioRxiv preprint doi: https://doi.org/10.1101/498980; this version posted December 17, 2018. The copyright holder for this preprint (which was not certified by peer review) is the author/funder. All rights reserved. No reuse allowed without permission.

with PBS over the course of 1-2 days. Next, we used secondary antibodies conjugated with fluorophores (1:200): Goat anti-Chicken, Alexa Fluor 488, A11039, Invitrogen, Eugene, OR, US; Goat anti-Mouse, AlexaFluor 647, A31571, Invitrogen, Eugene, OR, US; all were used in the same buffer solution as described for primary antibodies above and incubated in darkness at room temperature with gentle agitation for 3 days. After that time, samples were washed extensively with PBS at least 5 times over 1-2 days at room temperature. Finally, samples were incubated in the refractive index-matching solution (RIMS, refractive index = 1.47) consisting of 40 g of Histodenz (cat. D2158, Sigma-Aldrich, UK) dissolved in 30 ml of PBS, pH=7.5 with 0.01% sodium azide. 200 µl of RIMS was used per DRG. Samples were allowed to equilibrate in RIMS overnight in darkness. Before imaging samples were placed in fresh RIMS in custom-made glass slide chambers and covered with coverslips. DRG were ready to image 4 hrs after final equilibration in RIMS.

Samples were imaged with a Zeiss LSM 780 single-photon confocal upright microscope, equipped with EC Plan-Neofluar 10x 0.3 NA, Ph1 dry objective (w.d=5.3 mm, cat. 420341-9911, Zeiss, Germany) and laser lines: 488, 633 nm. Scans were taken with 2048x2048 pixel resolution, with 4-5 µm optical section typically spanning 400-700 µm of scanned depth (resulting in 100-150 planes) with auto Z brightness correction to ensure uniform signal intensity throughout the sample. Images were exported from Zen 2012 Blue Edition software (Carl Zeiss Microscopy GmbH, Germany). Next graphical representations, 3D-rendering, animations, maximal intensity projections within selected z-stacks and further analysis were obtained with open-source Fiji (ImageJ) equipped with appropriate plugins.

Statistics

Statistical analyses were performed using SPSS v25 (IBM, Armonk, NY). All data plotted represent mean ± SEM. Detailed description of the number of samples analysed and their meaning, together with values obtained from statistical tests can be found in each figure legend. Main effects from ANOVAs are expressed as an F-statistic and P value within brackets. Statistical differences in the neuronal responses from the GCaMP experiments, were determined using a 2-way repeated-measures analysis of variance (RM-ANOVA), where applicable with Bonferroni post hoc test. Kruskal–Wallis one-way analysis of variance test (K-W, one-way ANOVA) was used to analyse behavioural data for weight bearing. Data for body mass between Sham

bioRxiv preprint doi: https://doi.org/10.1101/498980; this version posted December 17, 2018. The copyright holder for this preprint (which was not certified by peer review) is the author/funder. All rights reserved. No reuse allowed without permission.

and CIBP groups was analysed by 2-way repeated-measures analysis of variance (RM-ANOVA) with Bonferroni post hoc test. One way ANOVA with Tukey post-hoc performed in GraphPad Prism, was used to analyse data in Figure 4 for BMD and quantification of Atf3.

Acknowledgments

We would like to acknowledge Professor Timothy Arnett (UCL) for the ability to use µCT scanner, and Dr. Lawrence Moon (KCL) for statistical advice. This work was supported by grant from the European Union's Horizon 2020 research and innovation programme under the Marie Skłodowska-Curie grant agreement No.642720 and by a strategic award from the Wellcome Trust (102645/Z/13/Z).

Author Contributions

M.W.K. designed and performed all the experiments, analysed data and wrote the manuscript;

K.I.C. performed GCaMP experiments and analysed data;

D.M.L. corrected the manuscript;

D.D. performed Atf3 IHC experiments and analysed data;

K.B. corrected the manuscript;

F.D. provided conceptual input on the manuscript, corrected the manuscript;

A.H.D. supervised the study, acquired funding;

S.B.M. conceived, designed, and supervised the study, corrected the manuscript, and acquired funding.

Declaration of Interests

The authors declare no competing interests.

bioRxiv preprint doi: https://doi.org/10.1101/498980; this version posted December 17, 2018. The copyright holder for this preprint (which was not certified by peer review) is the author/funder. All rights reserved. No reuse allowed without permission.

References

1. Clohisy, D. & Mantyh, P. Bone cancer pain. *Cancer* **1198,** 173–81 (2003).
2. Mantyh, P. W. Cancer pain and its impact on diagnosis, survival and quality of life. *Nat. Rev. Neurosci.* **7,** 797–809 (2006).
3. Mantyh, P. W., Clohisy, D. R., Koltzenburg, M. & Hunt, S. P. Molecular mechanisms of cancer pain. *Nat. Rev. Cancer* **2,** 201–209 (2002).
4. Nyquist, M. D. & Nelson, P. S. Anti-Depressant Therapy Brightens the Outlook for Prostate Cancer Bone Metastases. *Cancer Cell* **31,** 303–305 (2017).
5. Bloom, A. P. *et al.* Breast cancer-induced bone remodeling, skeletal pain, and sprouting of sensory nerve fibers. *J. Pain* **12,** 698–711 (2011).
6. Jimenez-Andrade, J. M. *et al.* Pathological sprouting of adult nociceptors in chronic prostate cancer-induced bone pain. *J. Neurosci.* **30,** 14649–56 (2010).
7. Ghilardi, J. R. *et al.* Administration of a tropomyosin receptor kinase inhibitor attenuates sarcoma-induced nerve sprouting, neuroma formation and bone cancer pain. *Mol. Pain* **6,** 87 (2010).
8. McCaffrey, G. *et al.* NGF blockade at early times during bone cancer development attenuates bone destruction and increases limb use. *Cancer Res.* **74,** 7014–23 (2014).
9. Jimenez-Andrade, J. M., Ghilardi, J. R., Castañeda-Corral, G., Kuskowski, M. A. & Mantyh, P. W. Preventive or late administration of anti-NGF therapy attenuates tumor-induced nerve sprouting, neuroma formation, and cancer pain. *Pain* **152,** 2564–74 (2011).
10. Hayakawa, Y. *et al.* Nerve Growth Factor Promotes Gastric Tumorigenesis through Aberrant Cholinergic Signaling. *Cancer Cell* **31,** 21–34 (2017).
11. Toda, M. *et al.* Neuronal system-dependent facilitation of tumor angiogenesis and tumor growth by calcitonin gene-related peptide. *Proc Natl Acad Sci U S A* **105,** 13550–13555 (2008).
12. Boilly, B., Faulkner, S., Jobling, P. & Hondermarck, H. Nerve Dependence: From Regeneration to Cancer. *Cancer Cell* **31,** 342–354 (2017).
13. Hunter, D. V *et al.* Sensory and Motor Systems Advillin Is Expressed in All Adult Neural Crest-Derived Neurons. **5,** 77–95 (2018).
14. Treweek, J. B. *et al.* Whole-body tissue stabilization and selective extractions via tissue-hydrogel hybrids for high-resolution intact circuit mapping and

bioRxiv preprint doi: https://doi.org/10.1101/498980; this version posted December 17, 2018. The copyright holder for this preprint (which was not certified by peer review) is the author/funder. All rights reserved. No reuse allowed without permission.

phenotyping. *Nat. Protoc.* **10,** 1860–1896 (2015).

15. Usoskin, D. *et al.* Unbiased classification of sensory neuron types by large-scale single-cell RNA sequencing. *Nat. Neurosci.* **18,** 145–153 (2014).
16. Zeisel, A. *et al.* Molecular Architecture of the Mouse Nervous System. *Cell* **174,** 999–1014.e22 (2018).
17. Medhurst, S. J. *et al.* A rat model of bone cancer pain. *Pain* **96,** 129–40 (2002).
18. Peters, C. M. *et al.* Tumor-induced injury of primary afferent sensory nerve fibers in bone cancer pain. *Exp. Neurol.* **193,** 85–100 (2005).
19. Chisholm, K. I., Khovanov, N., Lopes, D. M., Russa, F. La & McMahon, S. B. Large Scale in Vivo Recording of Sensory Neuron Activity with GCaMP6. *eNeuro* ENEURO.0417-17.2018 (2018). doi:10.1523/ENEURO.0417-17.2018
20. Kaan, T. K. Y. *et al.* Systemic blockade of P2X3 and P2X2/3 receptors attenuates bone cancer pain behaviour in rats. *Brain* **133,** 2549–2564 (2010).
21. Prato, V. *et al.* Functional and Molecular Characterization of Mechanoinsensitive “Silent” Nociceptors. *Cell Rep.* **21,** 3102–3115 (2017).
22. Lee, W. *et al.* Synergy between Piezo1 and Piezo2 channels confers high-strain mechanosensitivity to articular cartilage. *Proc. Natl. Acad. Sci.* **111,** E5114–E5122 (2014).
23. Gottlieb, P. A., Suchyna, T. M. & Sachs, F. Properties and Mechanism of the Mechanosensitive Ion Channel Inhibitor GsMTx4, a Therapeutic Peptide Derived from Tarantula Venom. *Current Topics in Membranes* (2007). doi:10.1016/S1063-5823(06)59004-0
24. Ivanusic, J. J. Size, neurochemistry, and segmental distribution of sensory neurons innervating the rat tibia. *J. Comp. Neurol.* **517,** 276–283 (2009).
25. Jimenez-Andrade, J. M. *et al.* A phenotypically restricted set of primary afferent nerve fibers innervate the bone versus skin: therapeutic opportunity for treating skeletal pain. *Bone* **46,** 306–13 (2010).
26. Nencini, S. & Ivanusic, J. J. The physiology of bone pain. How much do we really know? *Frontiers in Physiology* (2016). doi:10.3389/fphys.2016.00157
27. Hasegawa, H., Abbott, S., Han, B.-X., Qi, Y. & Wang, F. Analyzing Somatosensory Axon Projections with the Sensory Neuron-Specific Advillin Gene. *J. Neurosci.* **27,** 14404–14414 (2007).
28. Woo, S. H. *et al.* Piezo2 is the principal mechanotransduction channel for proprioception. *Nat. Neurosci.* **18,** 1756–1762 (2015).

bioRxiv preprint doi: https://doi.org/10.1101/498980; this version posted December 17, 2018. The copyright holder for this preprint (which was not certified by peer review) is the author/funder. All rights reserved. No reuse allowed without permission.

29. Zappia, K. J., O'Hara, C. L., Moehring, F., Kwan, K. Y. & Stucky, C. L. Sensory neuron-specific deletion of TRPA1 results in mechanical cutaneous sensory deficits. *Eneuro* **4,** ENEURO.0069-16.2017 (2017).
30. Nencini, S. & Ivanusic, J. Mechanically sensitive Aδ nociceptors that innervate bone marrow respond to changes in intra-osseous pressure. *J. Physiol.* **595,** 4399–4415 (2017).
31. Nencini, S. *et al.* Mechanisms of nerve growth factor signaling in bone nociceptors and in an animal model of inflammatory bone pain. *Mol. Pain* **13,** 174480691769701 (2017).
32. Urch, C. E., Donovan-Rodriguez, T. & Dickenson, A. H. Alterations in dorsal horn neurones in a rat model of cancer-induced bone pain. *Pain* **106,** 347–356 (2003).
33. Szczot, M. *et al.* Cell-Type-Specific Splicing of Piezo2 Regulates Mechanotransduction. *Cell Rep.* **21,** 2760–2771 (2017).
34. Ranade, S. S. *et al.* Piezo2 is the major transducer of mechanical forces for touch sensation in mice. *Nature* **516,** 121–125 (2014).
35. Prescott, S. A., Ma, Q. & De Koninck, Y. Normal and abnormal coding of somatosensory stimuli causing pain. *Nat. Neurosci.* **17,** 183–191 (2014).
36. Wang, F. *et al.* Sensory Afferents Use Different Coding Strategies for Heat and Cold. *Cell Rep.* **23,** 2001–2013 (2018).
37. Ma, Q. P. & Woolf, C. J. Progressive tactile hypersensitivity: An inflammation-induced incremental increase in the excitability of the spinal cord. *Pain* **67,** 97–106 (1996).
38. Gold, M. S. & Gebhart, G. F. Nociceptor sensitization in pain pathogenesis. *Nature medicine* **16,** 1248–57 (2010).
39. Tomotsuka, N. *et al.* Up-regulation of brain-derived neurotrophic factor in the dorsal root ganglion of the rat bone cancer pain model. *J. Pain Res.* **7,** 415–423 (2014).
40. Zimmermann, M. Ethical guidelines for investigations of experimental pain in conscious animals. *Pain* **16,** 109–10 (1983).

bioRxiv preprint doi: https://doi.org/10.1101/498980; this version posted December 17, 2018. The copyright holder for this preprint (which was not certified by peer review) is the author/funder. All rights reserved. No reuse allowed without permission.

Figure titles and legends

Figure 1. Many deep body CGRP afferents express little or no Advillin

(A) Representative images of lumbar 3 DRG immunostained for CGRP and Advillin (Avil) in the Fast Blue (FB) traced tibial afferents. Arrows indicate FB/CGRP double positive neurons. Scale bars, 100 µm

(B) Quantification of (A). Mean ± SEM percentage of neurons positive for selected markers in analysed L3 DRG from n=3 rats.

(C) Example PACT-cleared L3 DRG from Avil/eGFP mice (green), immunolabelled for CGRP (red). Scale bars, 200 µm.

See also Figure S1 and Movie S1, Movie S2.

Figure 2. Cancer progression affects bone innervation

(A) Example micro-computer tomography reconstructions of rat tibiae in early (day 7/8) and late (day 14/15) cancer stage, with corresponding sham-operated controls. Red arrows indicate trabecular bone lesions and white arrows indicate cortical bone lesions. Bottom panel shows a plantar representation of selected micro-scans as indicated by dotted lines in the top panel.

(B) Volumetric bone mineral density quantification from 114 reconstructed micro-scans (every 34 µm) per bone. Selected planes for analysis were chosen to cover the tumour growth area (see methods for details). Trabecular (top) and cortical (bottom) bone mineral density quantification in mg/cm^3. Each dot represents a single bone from a separate animal (n = 5-7 per group). Data represent the mean ± SEM. One Way ANOVA [group] with Tukey post-hoc test. # vs. Sham early, * vs. respective Sham, $ vs. CIBP early. *p < 0.05, **p < 0.01, ****p < 0.0001.

(C) Representative images selected from lumbar 3 DRG of IHC analysis of Atf3 and TubullinβIII protein expression in the Fast Blue (FB) traced tibial afferents. FB was injected a week before the cancer cells or vehicle (sham) implantation. Scale bars, 100 µm.

(D) Distribution of all FB+ afferents within analysed ipsilateral lumbar DRG (L2-L5). No FB positivity was noticed in the contralateral lumbar DRG (not shown).

bioRxiv preprint doi: https://doi.org/10.1101/498980; this version posted December 17, 2018. The copyright holder for this preprint (which was not certified by peer review) is the author/funder. All rights reserved. No reuse allowed without permission.

(E) Quantification of all FB+ afferents within L2-5 DRG, analysed as a percentage of all neurons therein (TubullinβIII). Early (E, day 7/8 post cancer cells implantation) and late (L, day 14/15 post cancer cells implantation) stage groups. Each dot represents an average count from 10-20 10 µm sections from separate animals (n = 3-6). Data represent the mean ± SEM. One Way ANOVA [group]: $F_{3, 17} = 0.0335$, $p = 0.992$.

(F) Quantification of all Atf3+ afferents within L2-5 DRG analysed as a percentage of all neurons therein (TubullinβIII). Analysed as in (E), data represent the mean ± SEM. One Way ANOVA [group] with Tukey post-hoc test. # vs. Sham early, * vs. Sham late, $ vs. CIBP late. *p < 0.05, **p < 0.01, ****p < 0.0001.

(G) Quantification of all Atf3+ afferents within L2-5 DRG analysed as a percentage of all tibial cavity neurons traced with FB. Analysed as in (E), data represent the mean ± SEM. One Way ANOVA [group]: $F_{3, 17} = 8.844$, $p < 0.001$ with Tukey post-hoc test. # vs. Sham early, * vs. Sham late, $ vs. CIBP late. **p < 0.01.

(H) Static weight bearing measurement of rear legs. Within a timepoint, each dot represents a single animal (n = 13-20 per group). Each measurement was taken as an average of 5 consecutive readouts per animal per timepoint. Data represent the mean ± SEM. Kruskal-Wallis for independent samples: $p < 0.05$ (sham), $p < 0.0001$ (CIBP): *p < 0.05, $^{\$\$}p < 0.01$, ***p < 0.0001; * vs. CIBP baseline (BL), $ vs. Sham baseline (BL).

See also Figure S2 and Movie S3.

Figure 3. DRG afferents encode mechanical pressure stimuli in a graded fashion

(A) Schematic representation of the GCaMP experiment. DRG, dorsal root ganglia; GCaMP, genetically encoded calcium indicator.

(B) Representative traces of GCaMP fluorescence during the knee compression with increased pressure. Sham-operated (left) and CIBP (right) murine model. Scale bars, 100 µm.

(C) Selected video frames of imaged DRG cell bodies responding to the knee compression and leg movements (Push/Pull along the body axis). Sham-operated (left) and CIBP (right) rat model. Scale bars, 100 µm.

bioRxiv preprint doi: https://doi.org/10.1101/498980; this version posted December 17, 2018. The copyright holder for this preprint (which was not certified by peer review) is the author/funder. All rights reserved. No reuse allowed without permission.

(D) Percentage of responders from 2507 neuronal cell bodies analysed from L3 and L4 DRG during the knee compression in Sham and CIBP animals. Pressure was increased in 50 mmHg steps every 10 s (See methods for more). Data represent the mean ± SEM (shaded areas) of n = 757 cells (sham) from 9 animals, and n = 1750 cells from 10 animals (CIBP). RM-ANOVA [group]: $F_{1, 2505} = 50.233$, $p < 0.0001$.

(E) Percentage of responders from 1337 neuronal cell bodies analysed from L3 and L4 DRG during the leg movement along the body axis in Sham and CIBP animals. For simplification, only first Pull/Push responses out of 5 consecutive pairs are presented (See for more in Fig. S4). Data represent the mean ± SEM (shaded areas) of n = 359 cells (sham) from 6 animals, and n = 978 cells from 6 animals (CIBP). RM-ANOVA [group]: $F_{1, 1335} = 31.338$, $p < 0.0001$.

See also Figure S3 and Movie S4.

Figure 4. CIBP appears to recruit previously silent nociceptive C fibres

(A) Intensities of all responding neuronal cell bodies from L3 and L4 DRG to the knee compression. Pressure was incrementally increased in 50 mmHg steps every 10 s. Data represent the mean ± SEM (shaded areas). N = 70 cells (sham) from 9 animals, and n = 421 cells from 10 animals (CIBP). RM-ANOVA [group]: $F_{1, 489} = 0.312$, $p = 0.577$.

(B) Intensities of all responding neuronal cell bodies from L3 and L4 DRG to the leg movement along the body axis. For simplification, only first Pull/Push responses out of 5 consecutive pairs are presented (See for more in Fig. S5). Data represent the mean ± SEM (shaded areas). N = 81 cells (sham) from 6 animals, and n = 487 cells from 6 animals (CIBP). RM-ANOVA [group]: $F_{1, 566} = 0.107$, $p = 0.744$.

(C) Cell size analysis of all responders during the knee compression in Sham and CIBP animals. Pressure was incrementally increased in 50 mmHg steps every 10 s. Data represent the mean ± SEM (shaded areas). N = 39 cells (sham) from 9 animals, and n = 165 cells from 10 animals (CIBP). RM-ANOVA [group]: $F_{1, 202} = 16.24$, ****$p < 0.0001$.

(D) Cell size analysis of all responders during the leg movement along the body axis in Sham and CIBP animals. For simplification, presented only first

bioRxiv preprint doi: https://doi.org/10.1101/498980; this version posted December 17, 2018. The copyright holder for this preprint (which was not certified by peer review) is the author/funder. All rights reserved. No reuse allowed without permission.

Pull/Push responses out of 5 consecutive pairs (See for more in Fig. S5). Data represent the mean ± SEM (shaded areas). N = 50 cells (sham) from 9 animals, and n = 255 cells from 10 animals (CIBP). RM-ANOVA [group]: $F_{1, 303} = 0.239$, $p = 0.625$.

(E) Left panels depict cell size distributions in sham (top) and CIBP (bottom) of all responders to different stimuli. Green lines highlight cell size separators used: <700 µm^2 (small cells), >700<1200 µm^2 (medium cells). Right panels show a summary count of responders to the increased knee compression within each cell size range. Sham (top), CIBP (bottom).

See also Figure S4 and Movie S4.

Figure 5. Intratibial afferent function in health and CIBP

(A) Schematic representation of the GCaMP experiment with traced intratibial (Fast Blue) afferents. FB, fast blue; DRG, dorsal root ganglia; GCaMP, genetically encoded calcium indicator.

(B) Summary of the total cell numbers and animals analysed in this experiment.

(C) Representative z-stack collected at the end of experiment in order to identify traced cells. Scale bars: 100 µm.

(D) Representative images of traced tibial afferents in L3 DRG collected after the GCaMP experiments. Sliced DRG were immunostained for Piezo2 (top) and TrkA (bottom). Scale bars: 50 µm.

(E) Percentage of responders of all FB-traced tibial afferents within L3 and L4 DRG during the knee compression in sham and CIBP animals. Pressure was increased in 50 mmHg steps every 10 s (See methods for more). Data represent the mean ± SEM (shaded areas) of N = 85 cells from 6 animals (sham) and 230 cells from 9 animals (CIBP). RM-ANOVA [group]: $F_{1, 313} = 0.286$, $p = 0.593$.

(F) Percentage of responders of all FB-traced tibial afferents within L3 and L4 DRG during the leg movement along the body axis in Sham and CIBP animals. For simplification, only first Pull/Push responses out of 5 consecutive pairs are presented (See for more in Fig. S6). Data represent the mean ± SEM (shaded areas) of N = 54 cells from 4 animals (sham) and 157 cells from 6 animals (CIBP). RM-ANOVA [group]: $F_{1, 209} = 0.037$, $p = 0.848$.

bioRxiv preprint doi: https://doi.org/10.1101/498980; this version posted December 17, 2018. The copyright holder for this preprint (which was not certified by peer review) is the author/funder. All rights reserved. No reuse allowed without permission.

(G) Intensities of all responding FB+ neuronal cell bodies to the knee compression. Pressure was incrementally increased in 50 mmHg steps every 10 s. Data represent the mean ± SEM (shaded areas). N = 15 cells (sham) from 6 animals, and n = 37 cells from 9 animals (CIBP). RM-ANOVA [group]: $F_{1, 50} = 0.577$, $p = 0.451$.

(H) Intensities of all responding FB+ neuronal cell bodies to the leg movement along the body axis. For simplification, only first Pull/Push responses out of 5 consecutive pairs are presented (See for more in Fig. S6). Data represent the mean ± SEM (shaded areas). N = 14 cells (sham) from 4 animals, and n = 70 cells from 6 animals (CIBP). RM-ANOVA [group]: $F_{1, 82} = 8.507$, $p < 0.01$.

See also Figure S5.

Figure 6. Muscle and periosteum afferents are recruited and sensitized by bone cancer

(A) Schematic representation of the GCaMP experiment with traced (AAVrg/dTomato) muscle and tibial periosteum (MP) afferents. DRG, dorsal root ganglia; GCaMP, genetically encoded calcium indicator.

(B) Summary of the total cell numbers and animals analysed in this experiment.

(C) Representative z-stack collected at the end of experiment in order to identify traced cells. Scale bars: 100 µm.

(D) Representative images of traced MP afferents in L3 DRG collected after the GCaMP experiments. Sliced DRG were immunostained for Piezo2 (top) and TrkA (bottom). tdTomato (MP afferents) is blue coded for clarity. Scale bars: 50 µm.

(E) Percentage of responders of all traced MP afferents within L3 and L4 DRG during the knee compression in sham and CIBP animals. Pressure was increased in 50 mmHg steps every 10 s (See methods for more). Data represent the mean ± SEM (shaded areas) of N = 11 cells from 3 animals (sham) and 43 cells from 5 animals (CIBP). RM-ANOVA [group]: $F_{1, 52} = 3.077$, $p = 0.085$.

(F) Intensities of all responding MP afferents to the knee compression. Pressure was incrementally increased in 50 mmHg steps every 10 s. Data represent the mean ± SEM (shaded areas) of N = 9 cells from 5 animals

bioRxiv preprint doi: https://doi.org/10.1101/498980; this version posted December 17, 2018. The copyright holder for this preprint (which was not certified by peer review) is the author/funder. All rights reserved. No reuse allowed without permission.

(CIBP). Statistical analysis was not performed as there were no response intensity values in the sham group.

See also Figure S6.

Figure 7. Pharmacological block of Piezo2 inhibits activated silent nociceptors

(A) Schematic representation of the experiment. In total 10 µg of GsMTx4 toxin (Piezo2 blocker) in 50 µl of saline was injected intramuscularly on each side (25 ul per site) of the cancer-bearing tibia. DRG, dorsal root ganglia; GCaMP, genetically encoded calcium indicator.

(B) Selected video frames of imaged DRG cell bodies responding to the knee compression before (0 min), 20 min and 40 min after the toxin injection. Sham-operated (left) and CIBP (right) rat model. Scale bars, 100 µm.

(C) Percentage of responders from 564 neuronal cell bodies analysed from L3 DRG during the knee compression in CIBP animals, before and after toxin injection. Pressure was increased in 50 mmHg steps every 10 s (See methods for more). Data represent the mean ± SEM (shaded areas) of N = 546 cells from 3 animals. RM-ANOVA [time]: $F_{2, 1689} = 6.704$, $p < 0.001$ with Bonferroni post hoc: 40 min. vs. Baseline $P < 0.007$, 40 min. vs. 20 min. $P < 0.003$. Dotted lines represent a total number of responders from all experiments in sham and CIBP groups (presented in detailed in Fig.4).

(D) Intensities of all responding neuronal cell bodies analysed to the knee compression before and after the toxin injection. Pressure was incrementally increased in 50 mmHg steps every 10 s. Data represent the mean ± SEM (shaded areas). N = 149 cells from 3 animals. RM-ANOVA [time]: $F_{2, 447} = 1.739$, $p = 0.177$.

(E) Schematic representation of the suggested mechanism of recruitment of silence nociceptors in cancer-induced bone pain rat model (explanation in text).

A

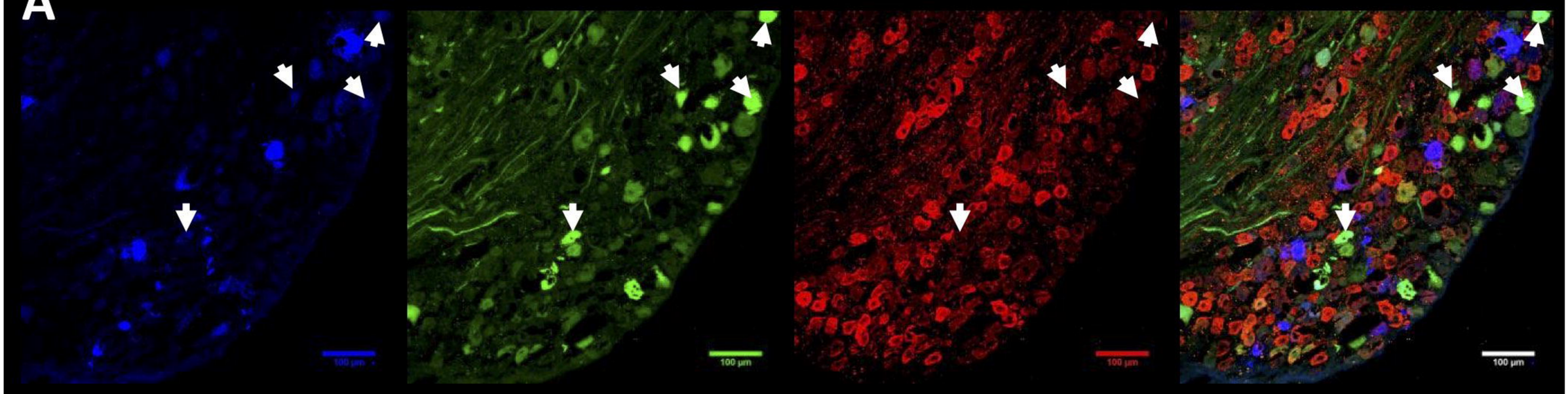

FB (tibia) CGRP Avil Merged

B

	% of FB+	% of CGRP+	% of Avil+
FB+ (516)		**49.54** ± 0.5	**15.19** ± 1.54
CGRP+ (753)	**72.29** ± 0.34		**23.68** ± 1.74
Avil+ (2014)	**59.30** ± 0.40	**63.35** ± 0.65	
CGRP+/Avil+ (477)	**45.93** ± 0.46	**31.47** ±0.67	**11.77** ± 6.71

C

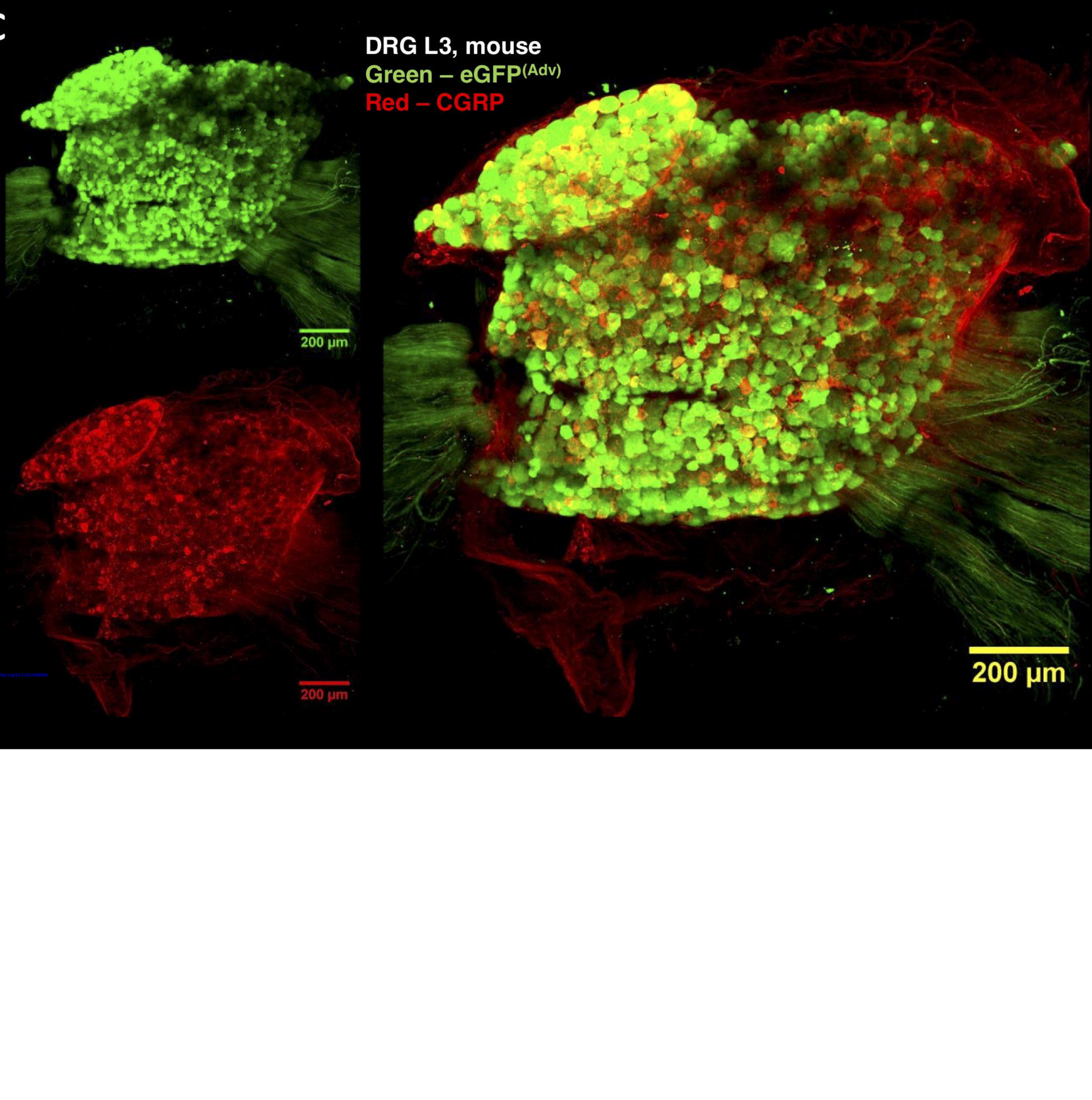

bioRxiv p https://doi.org/10.1101/498980 Posted December 18, 2018

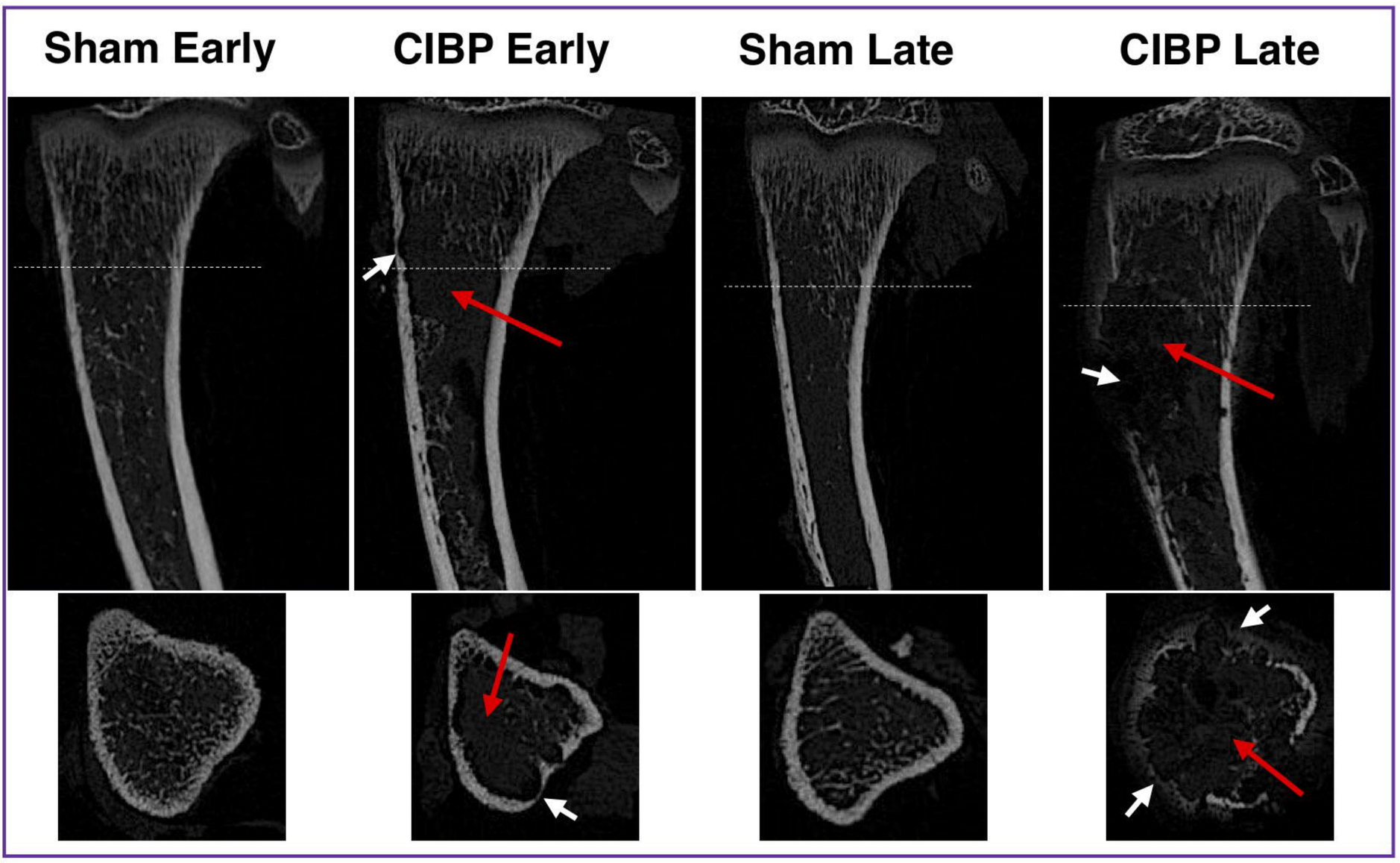

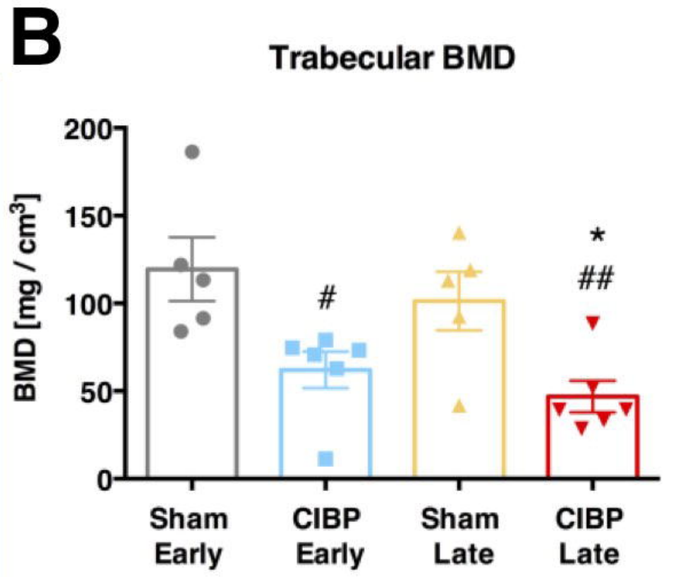

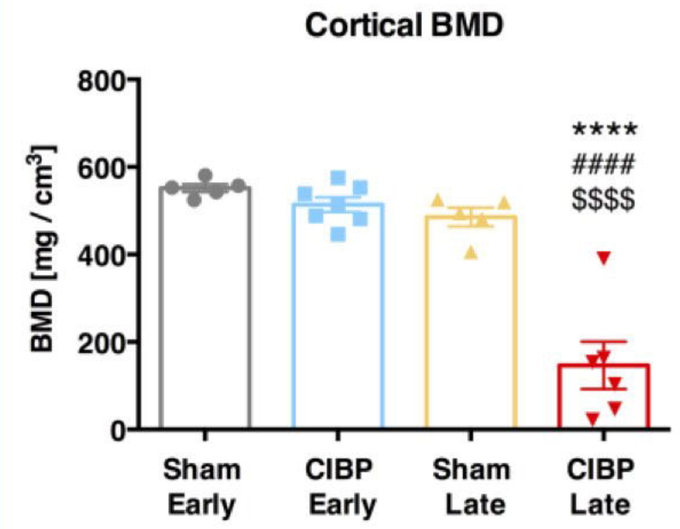

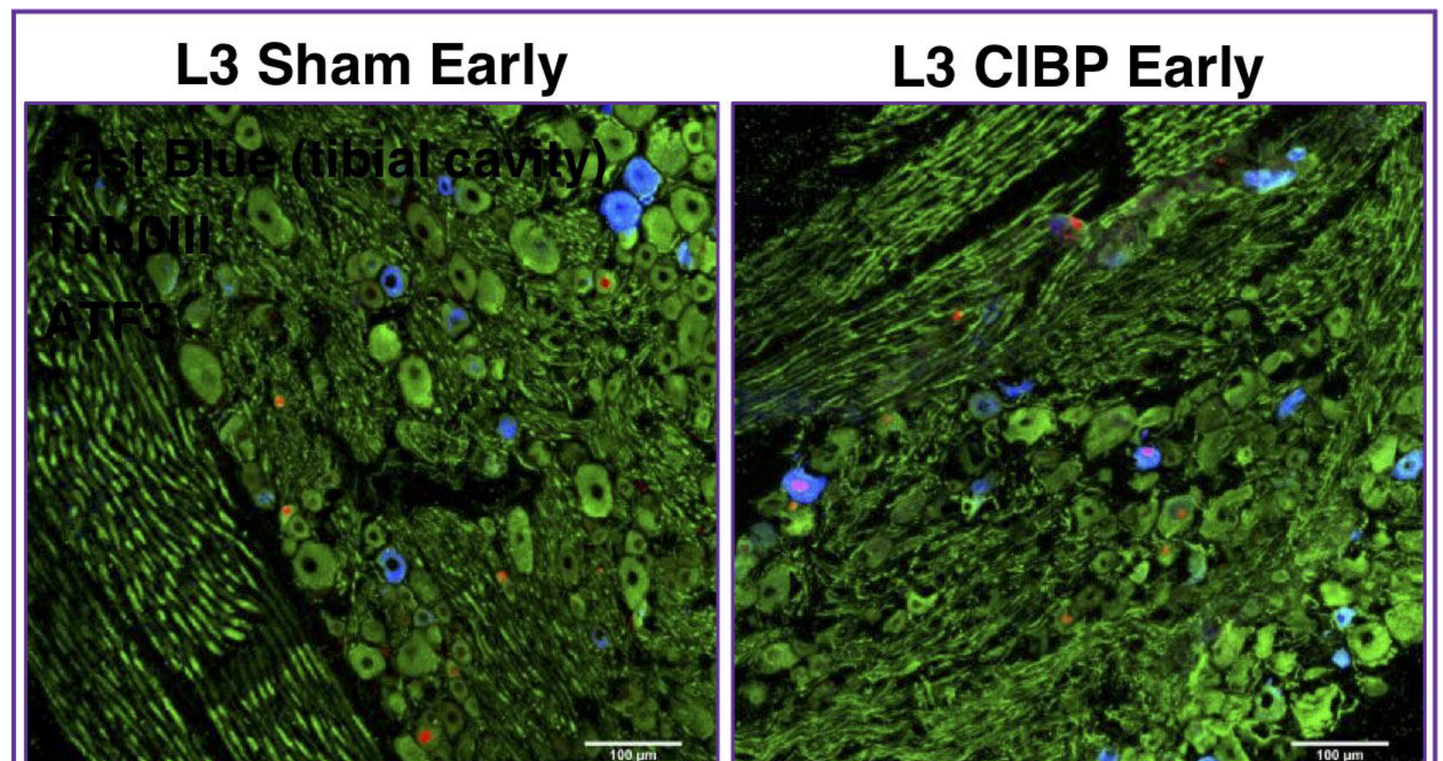

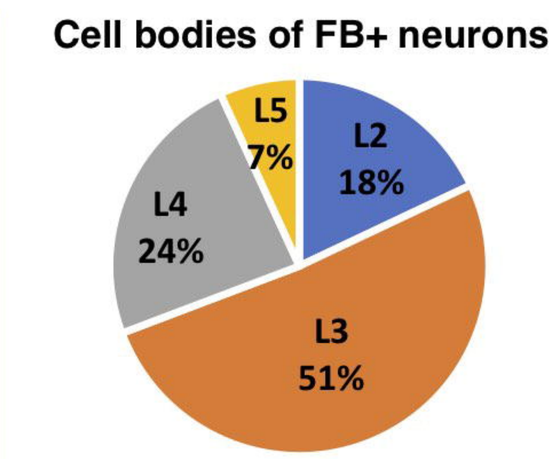

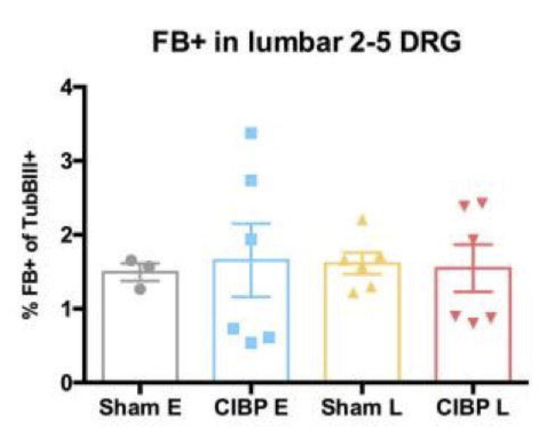

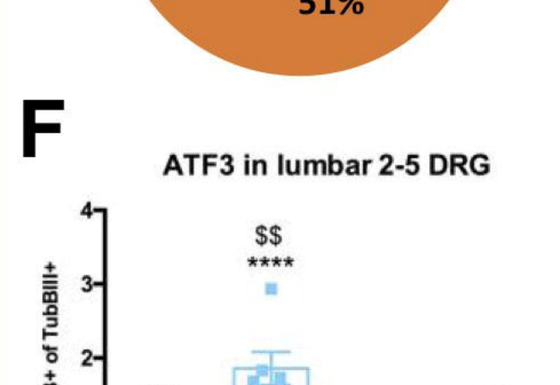

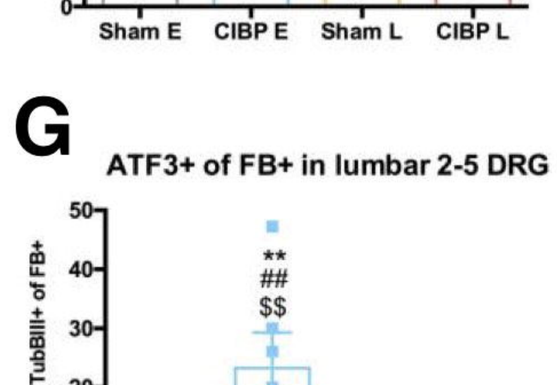

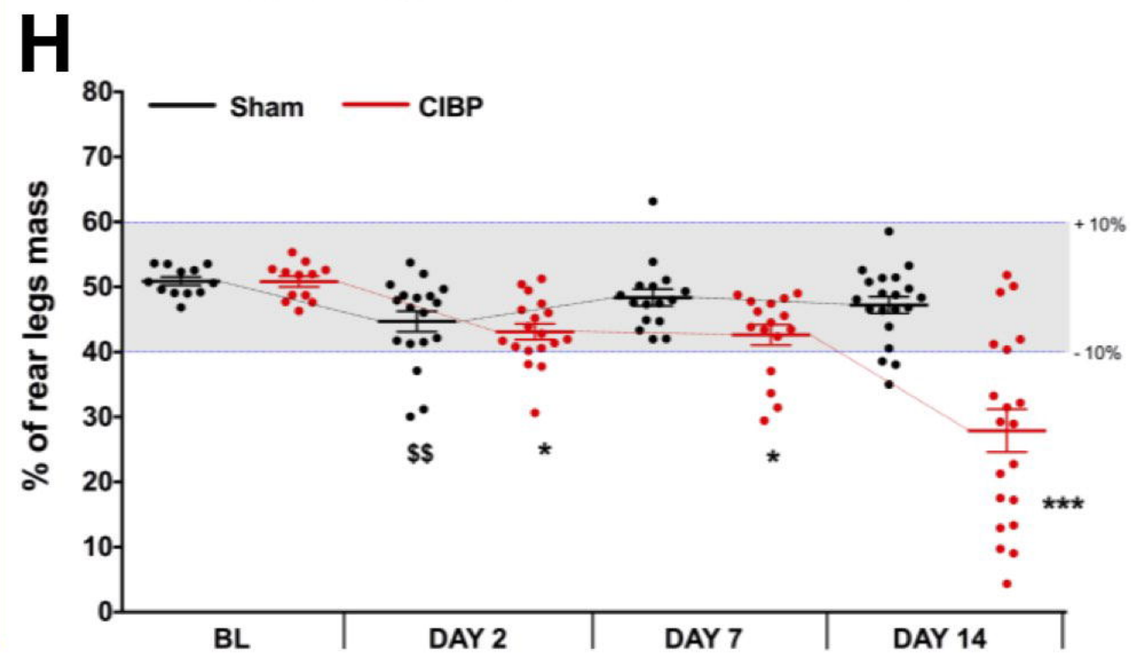

doi: https://doi.org/10.1101/868067 this version posted December 17, 2019. The copyright holder for this preprint (which was not certified by peer review) is the author/funder. All rights reserved. No reuse allowed without permission.

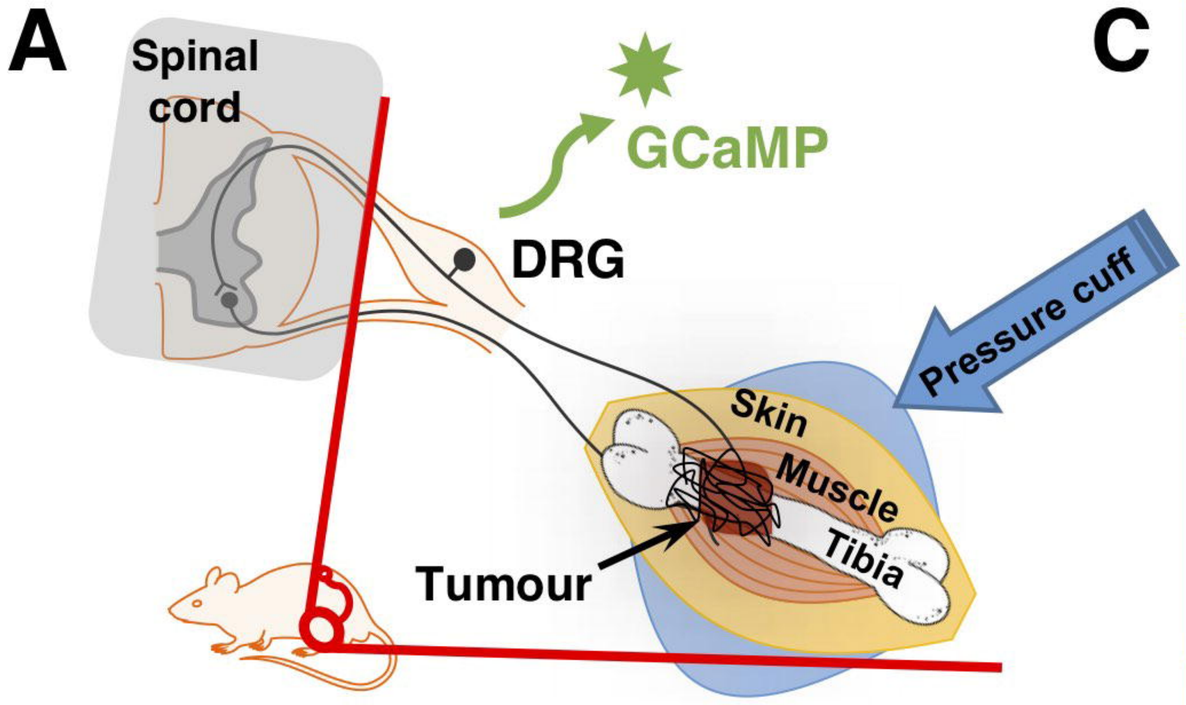

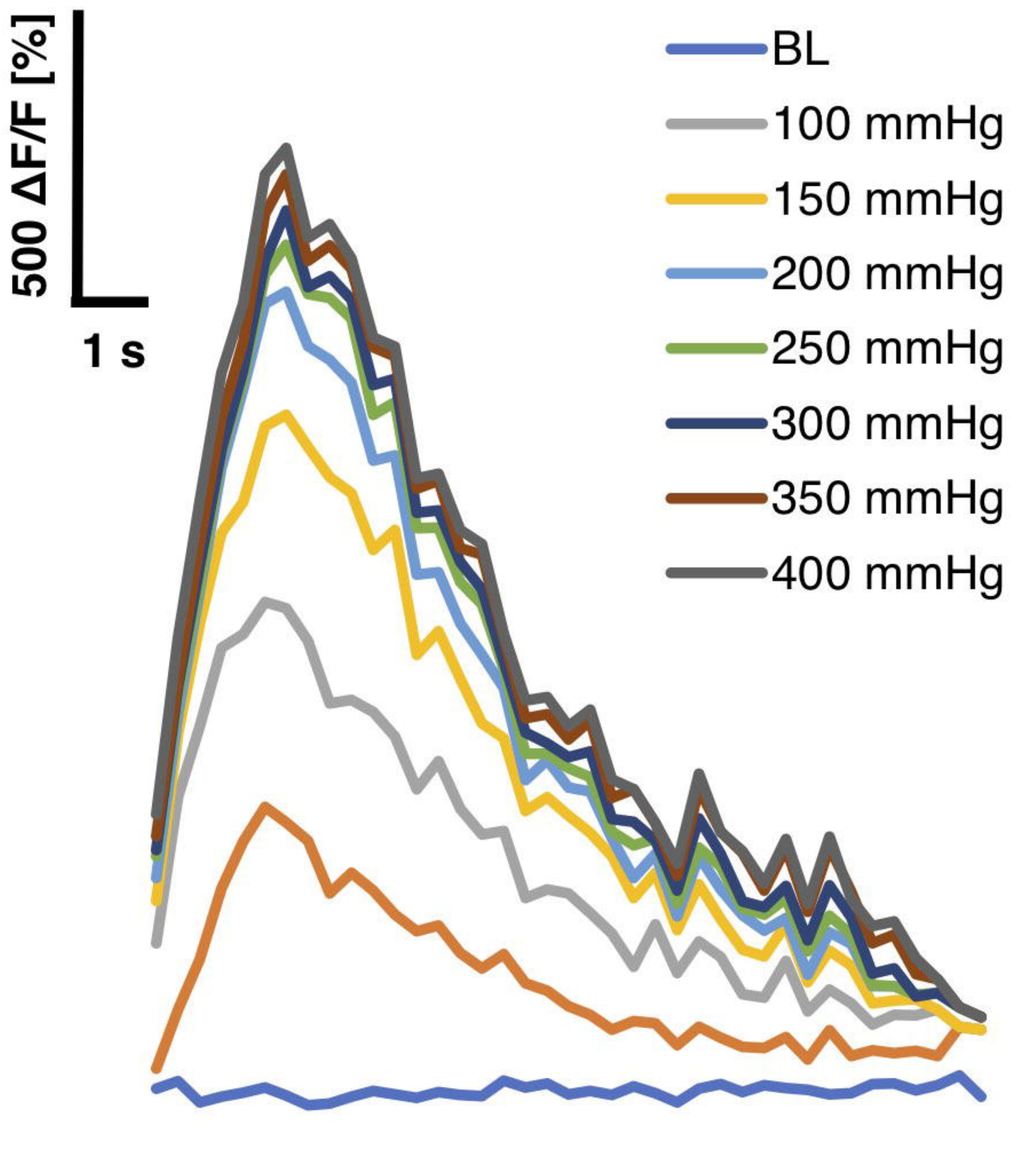

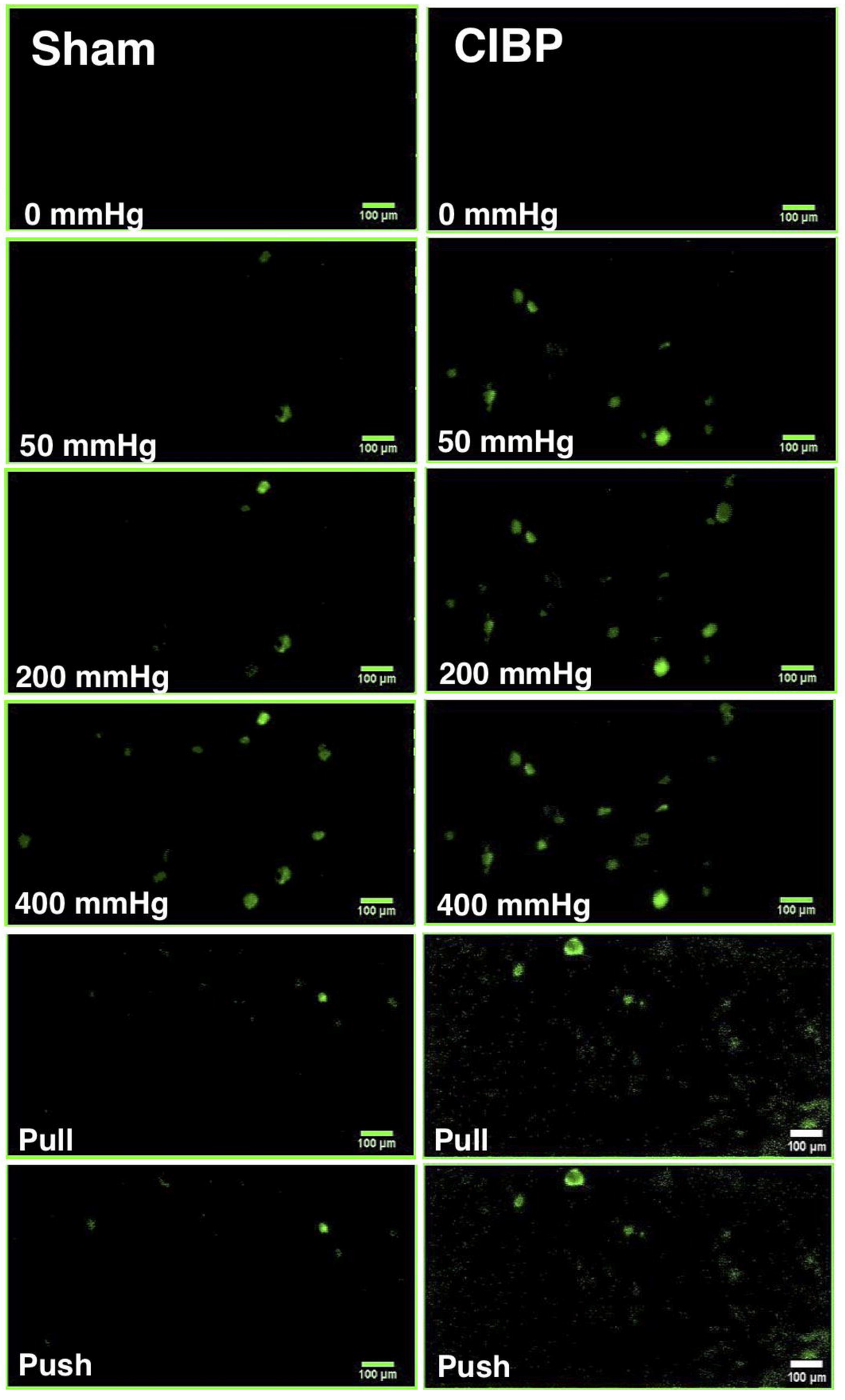

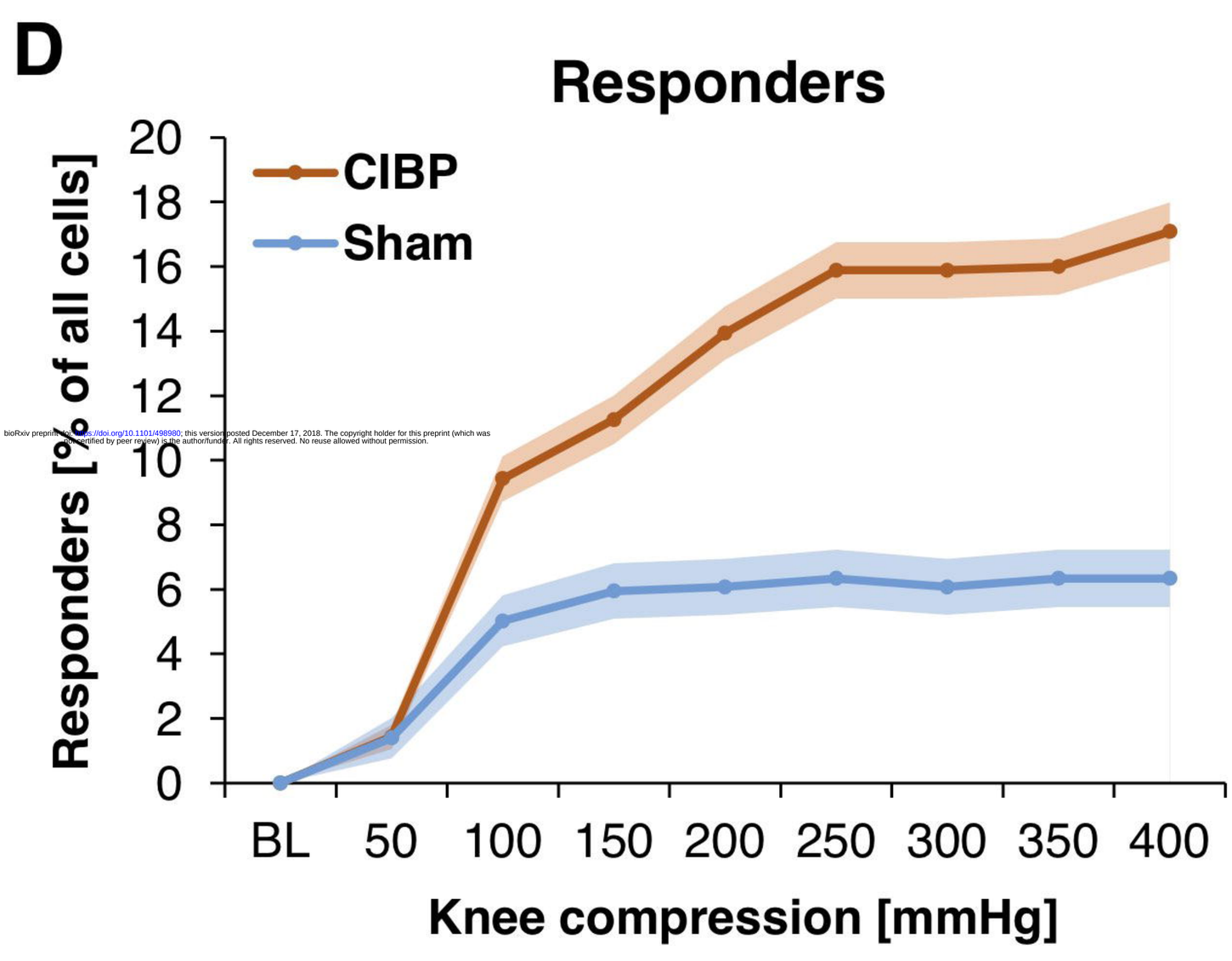

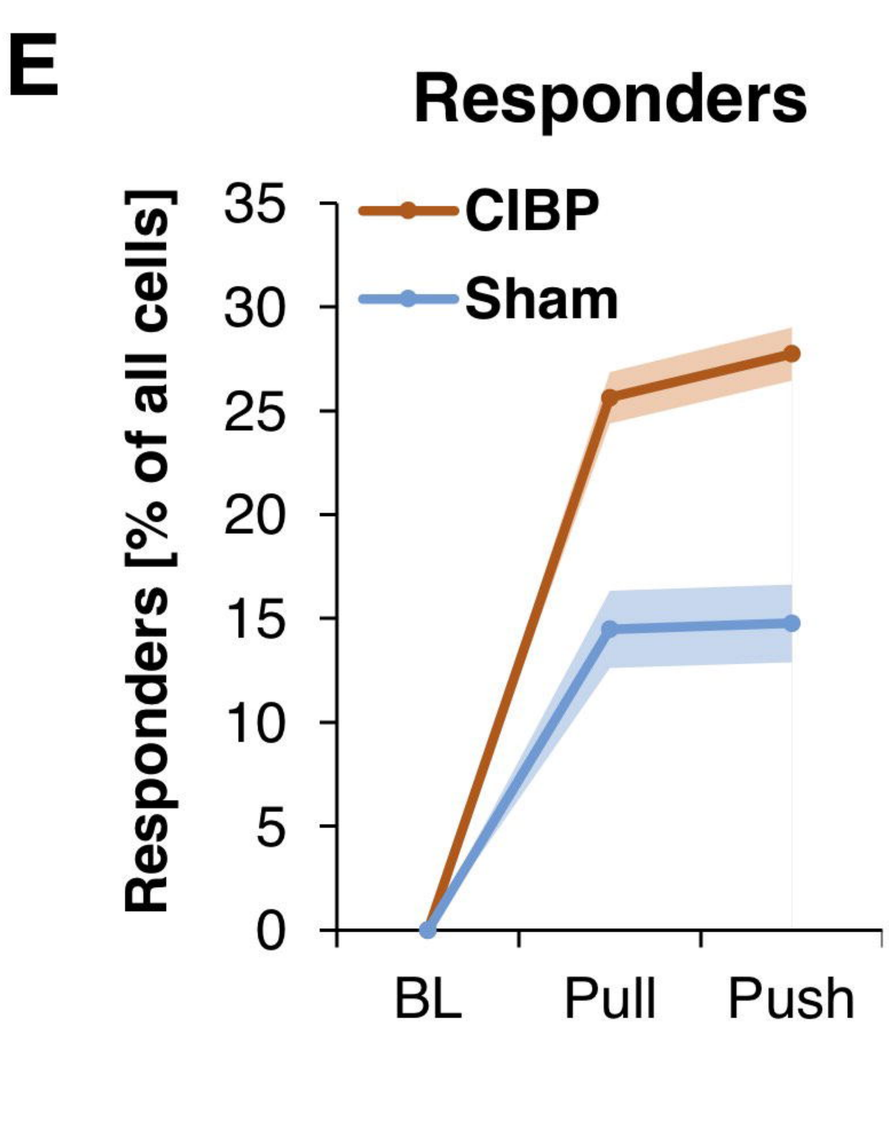

bioRxiv preprint doi: https://doi.org/10.1101/498980; this version posted December 17, 2018. The copyright holder for this preprint (which was not certified by peer review) is the author/funder. All rights reserved. No reuse allowed without permission.

bioRxiv preprint doi: https://doi.org/10.1101/498980; this version posted December 17, 2018. The copyright holder for this preprint (which was not certified by peer review) is the author/funder. All rights reserved. No reuse allowed without permission.

A

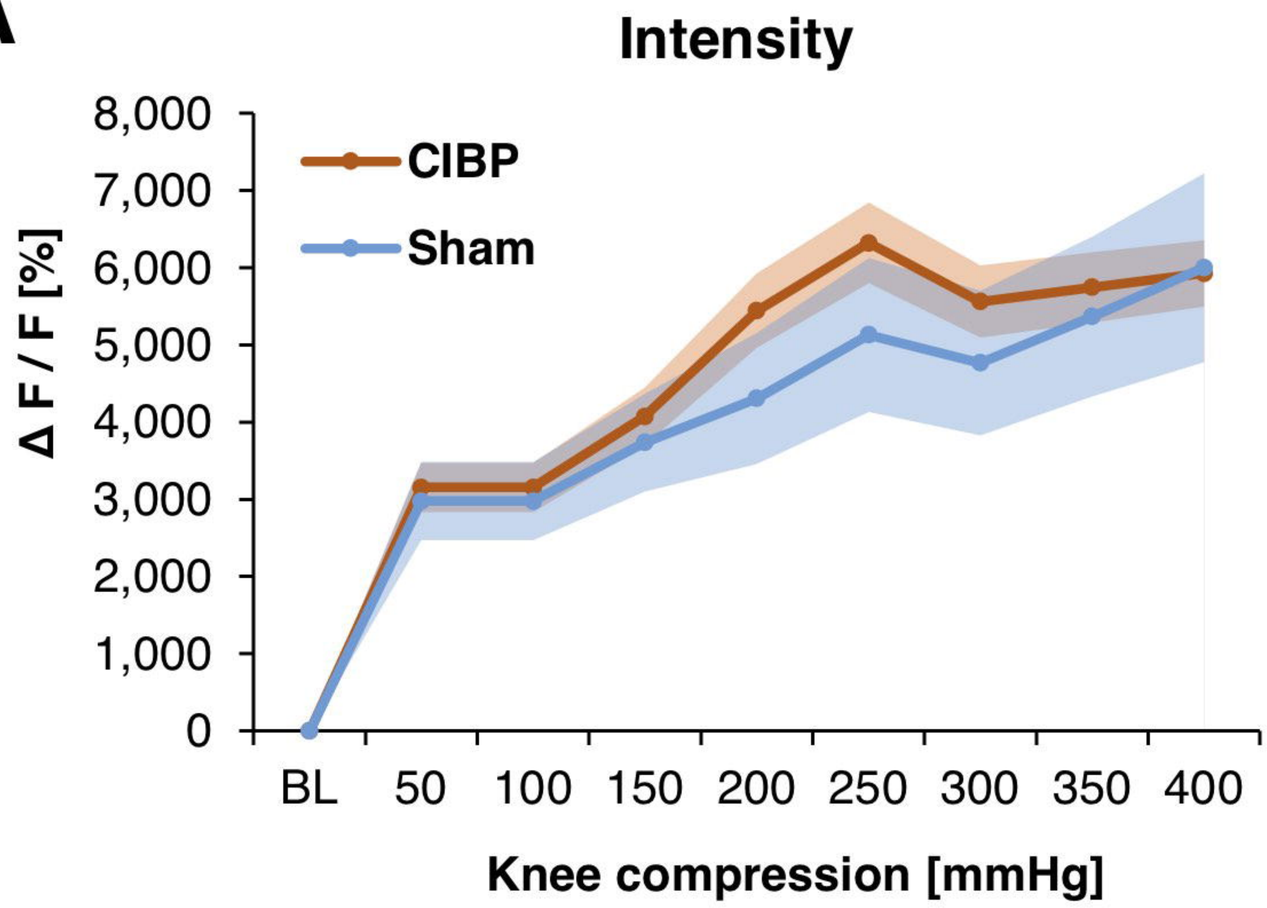

B

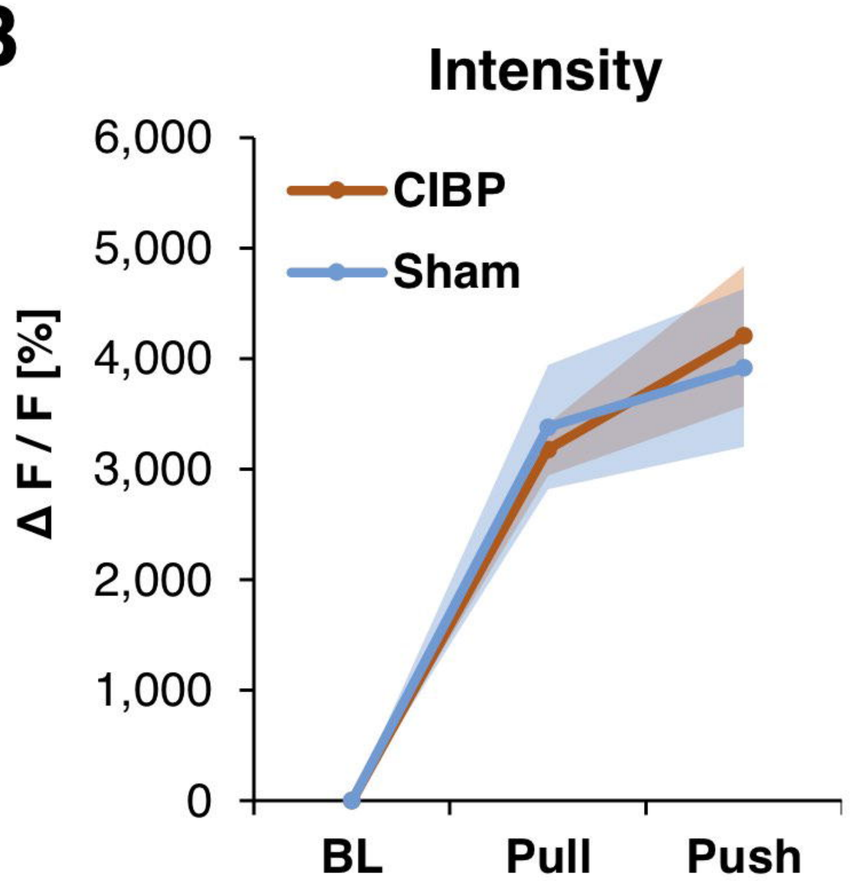

C

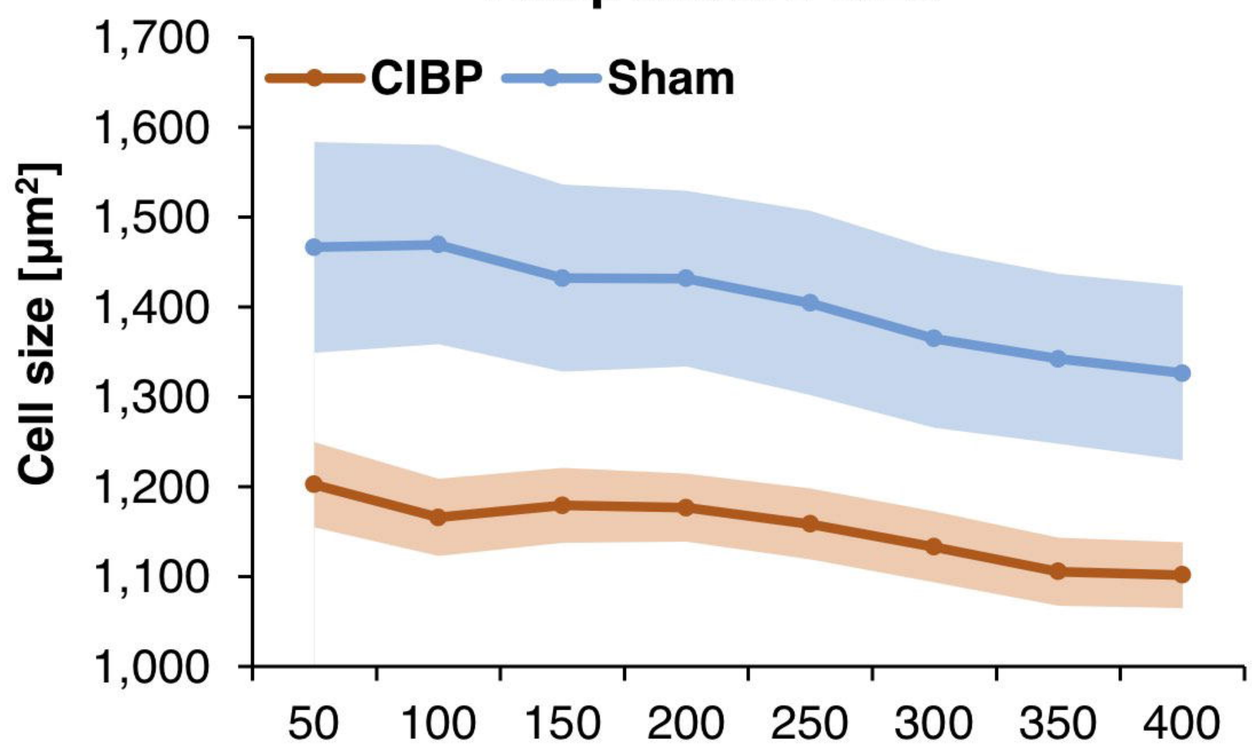

D

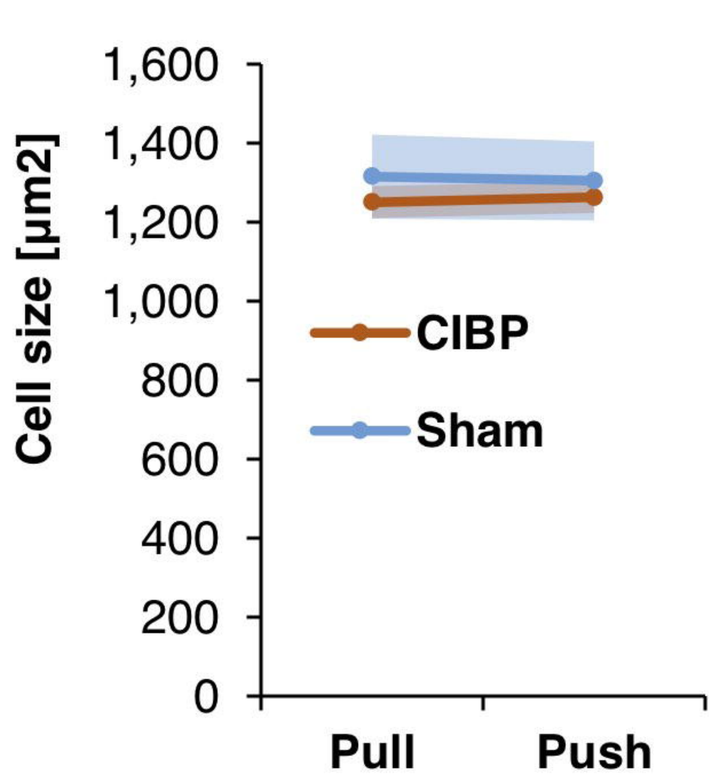

E

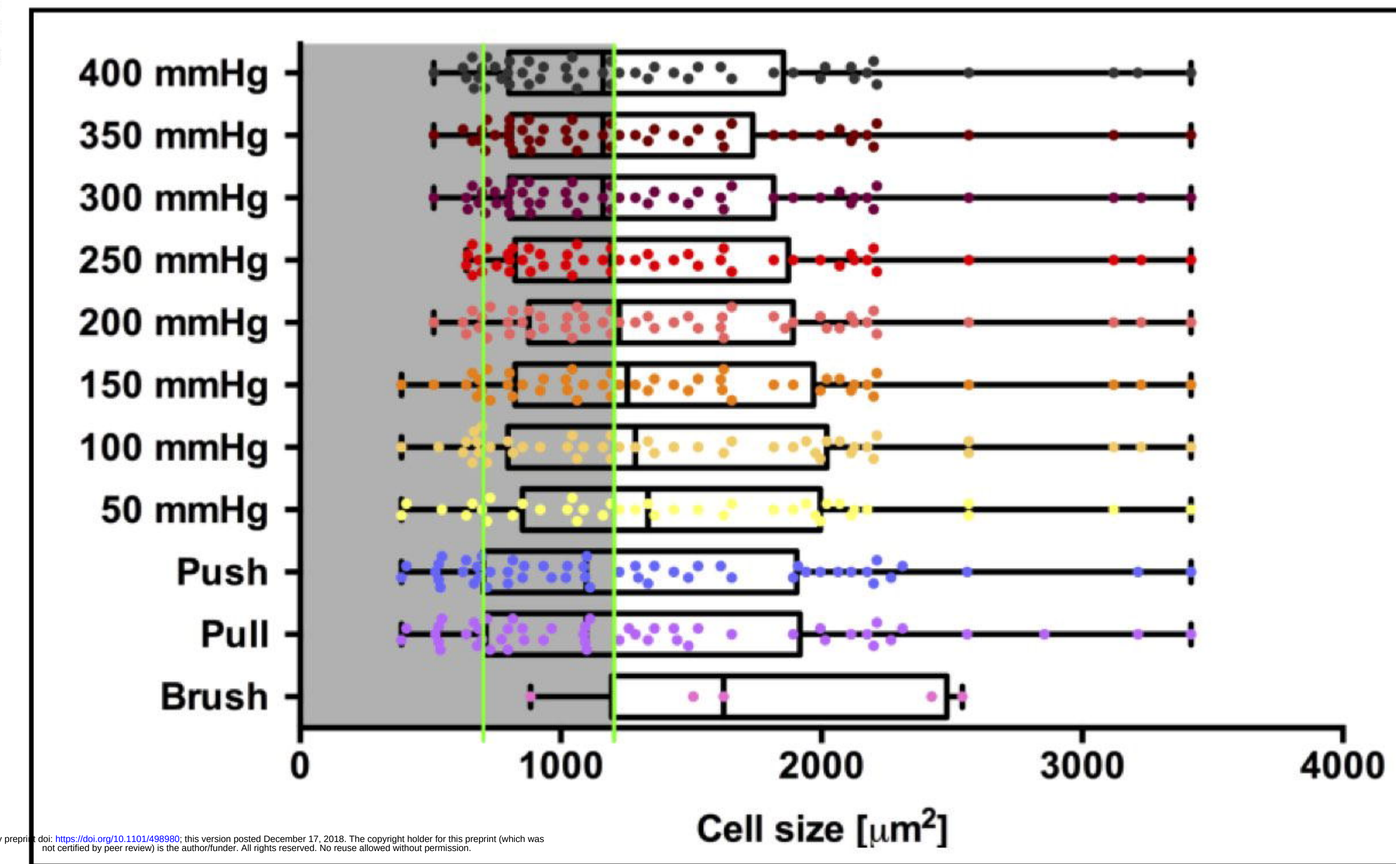

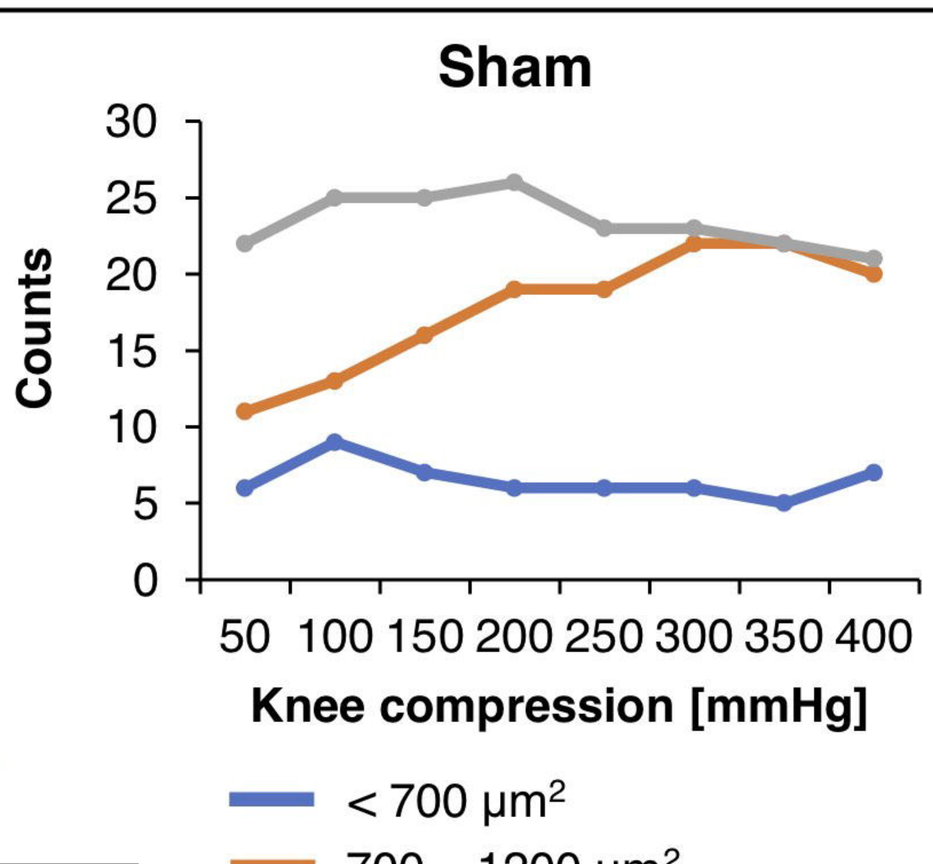

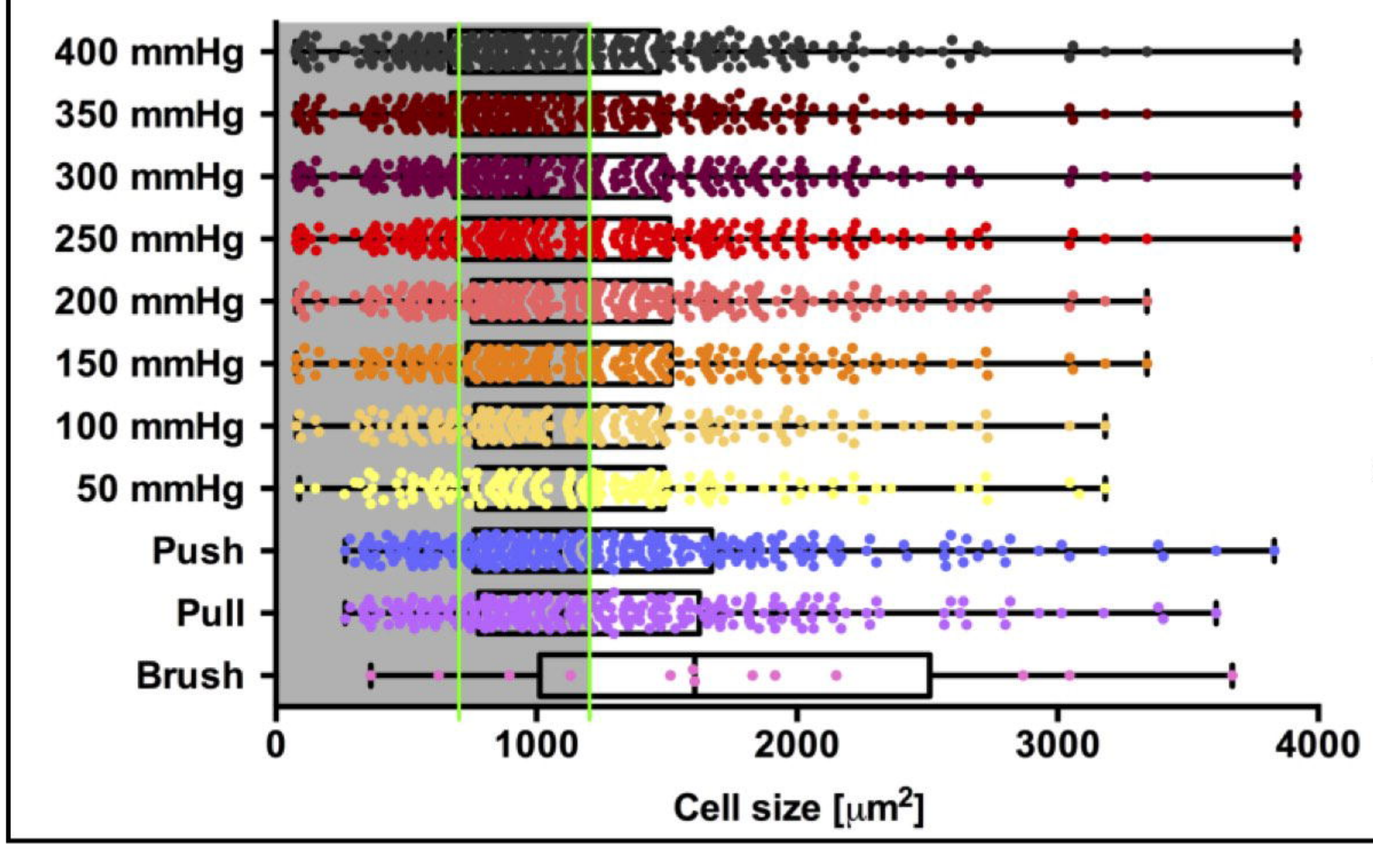

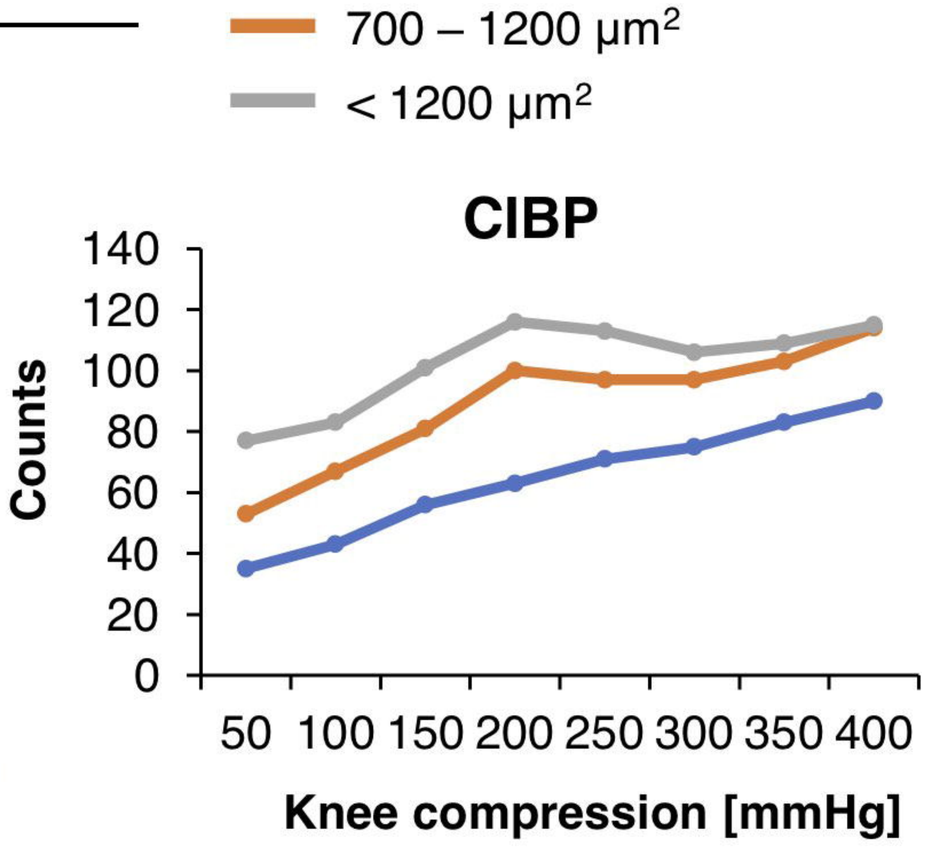

A

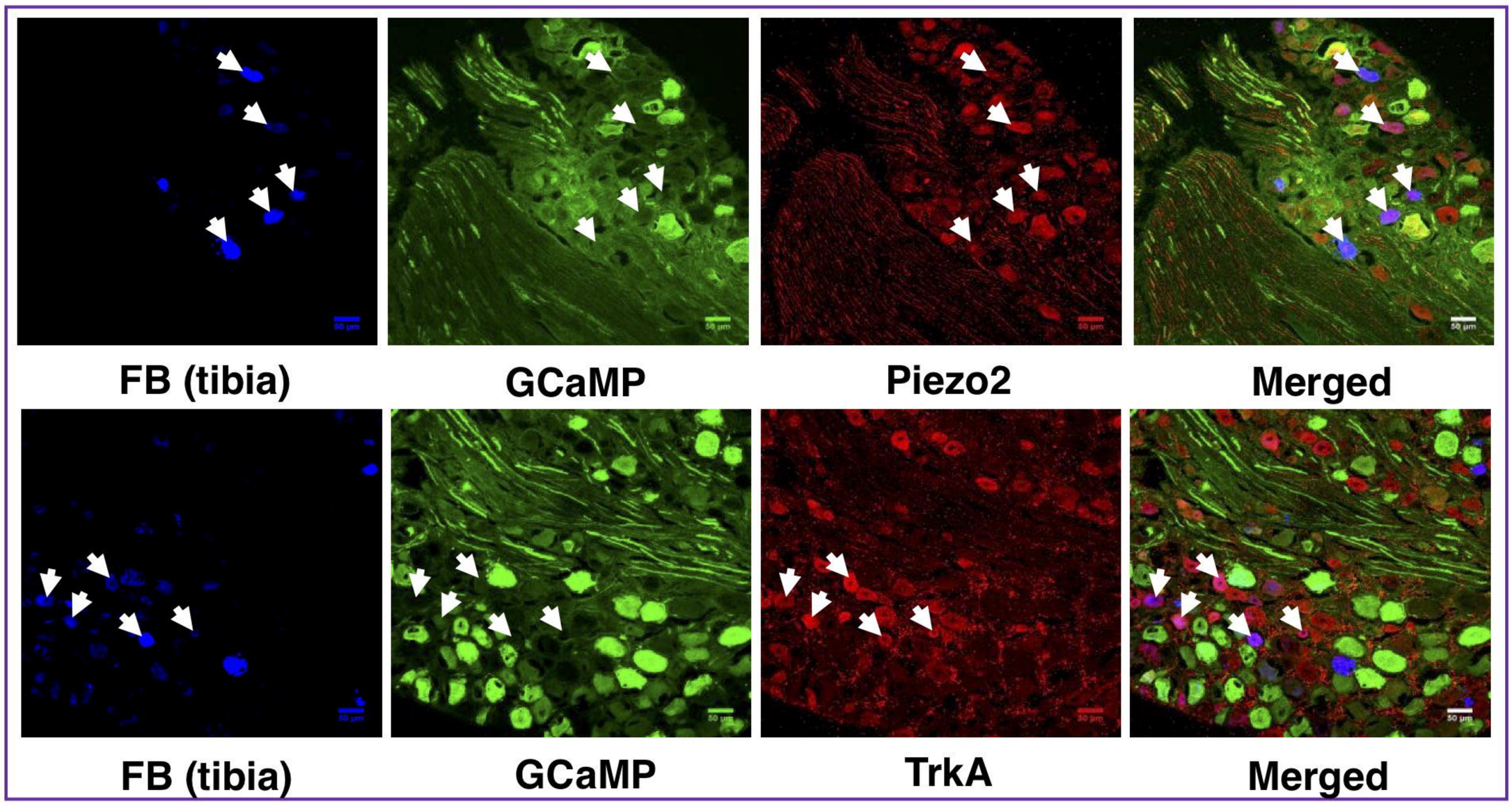

B

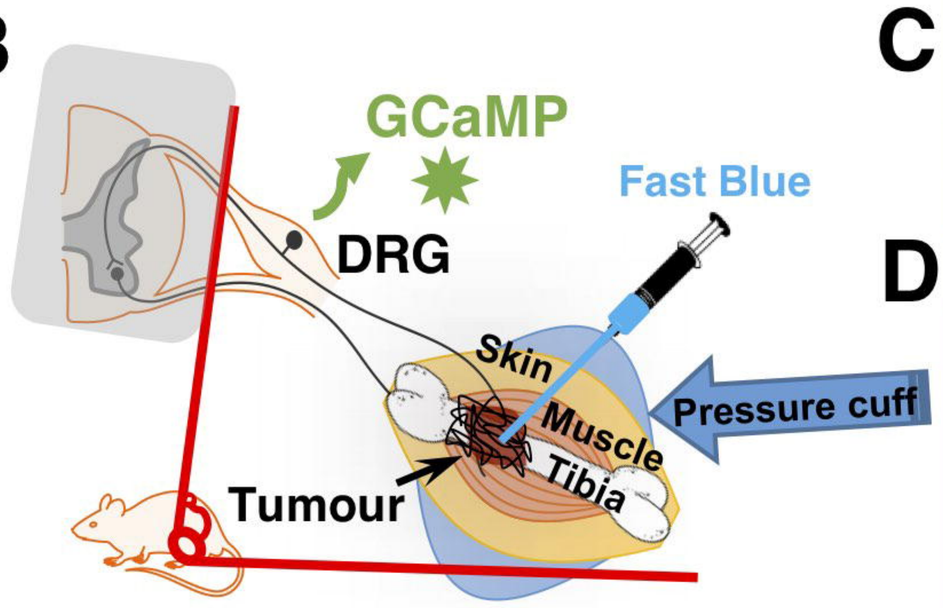

C

Number of cells (number of animals)	Sham	CIBP	Sum
Total (GCaMP+)	757 (9)	1750 (10)	2507 (19)
Bone (FB+)	83 (6)	234 (9)	317 (15)

D

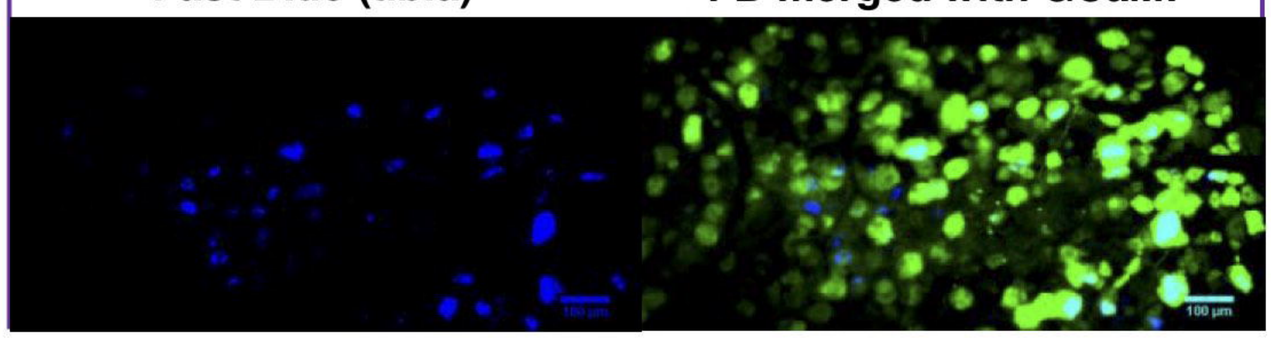

E

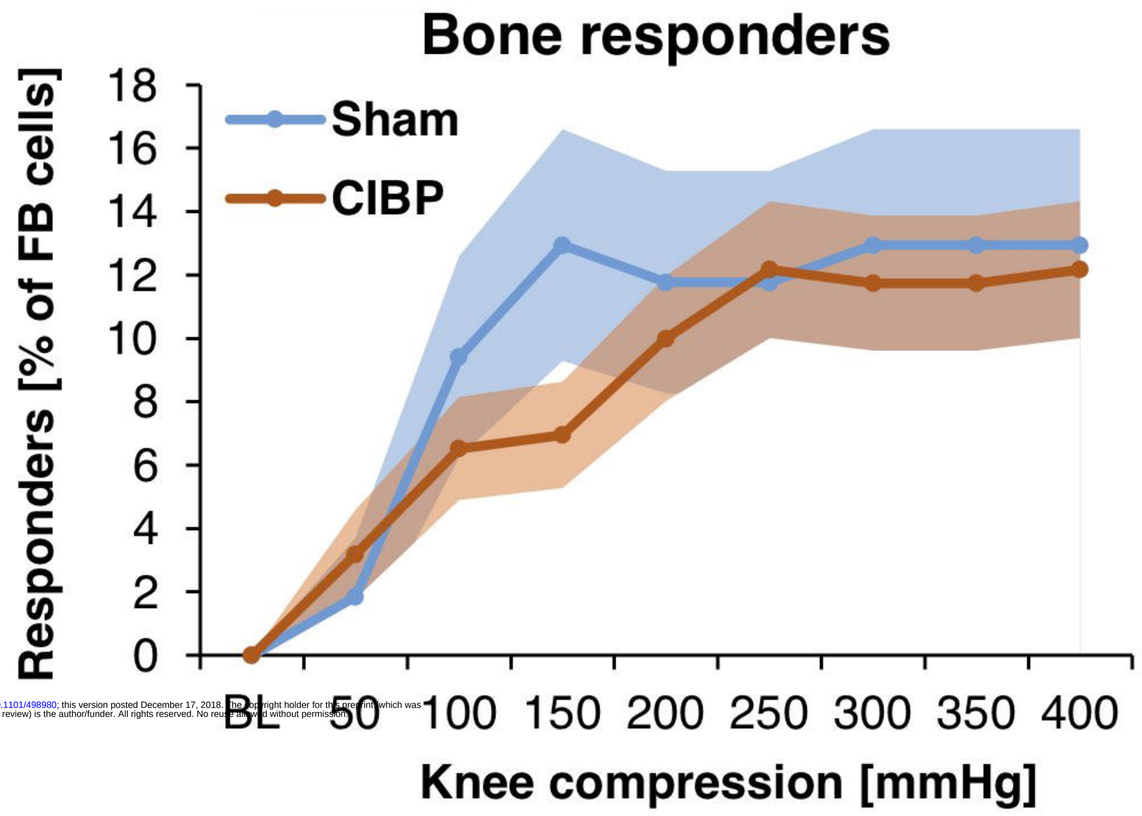

F

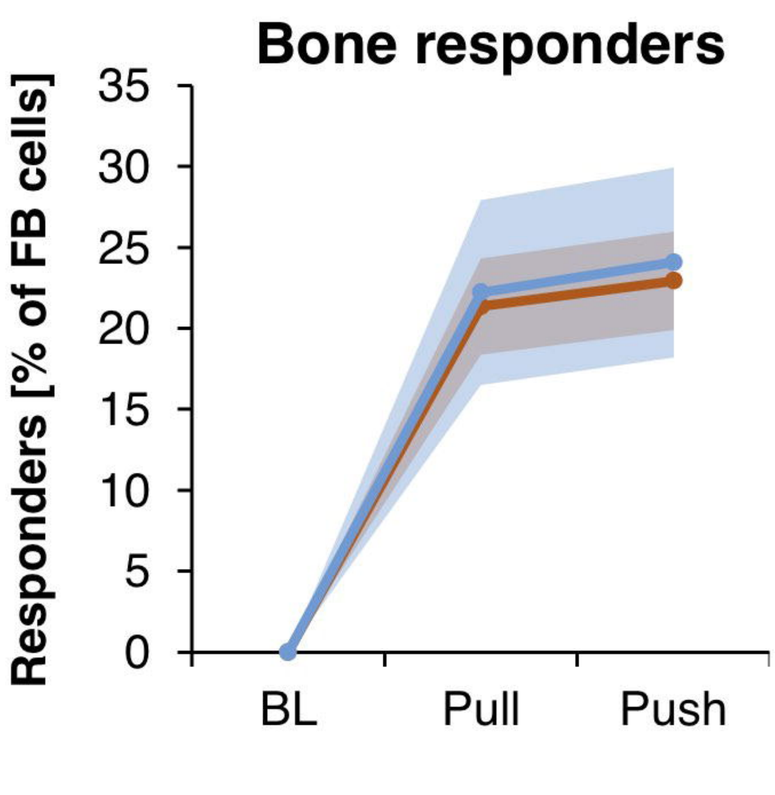

G

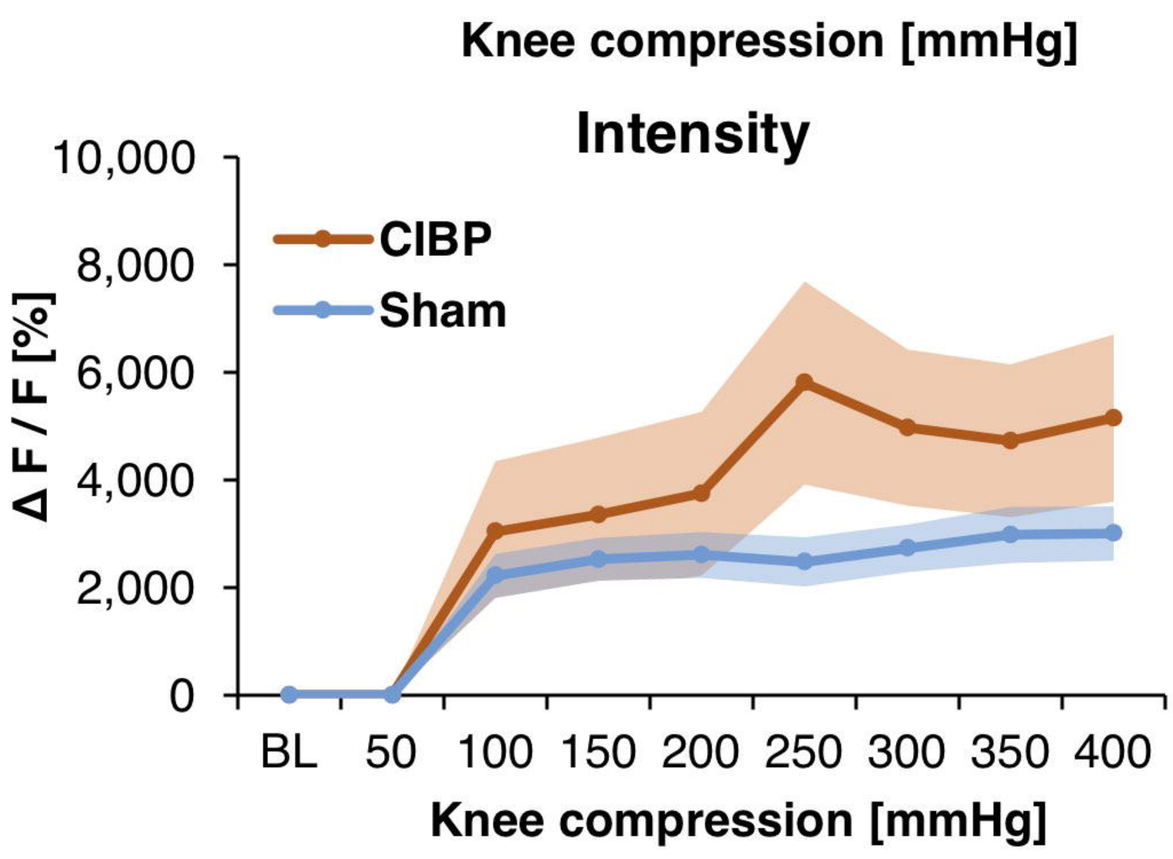

H

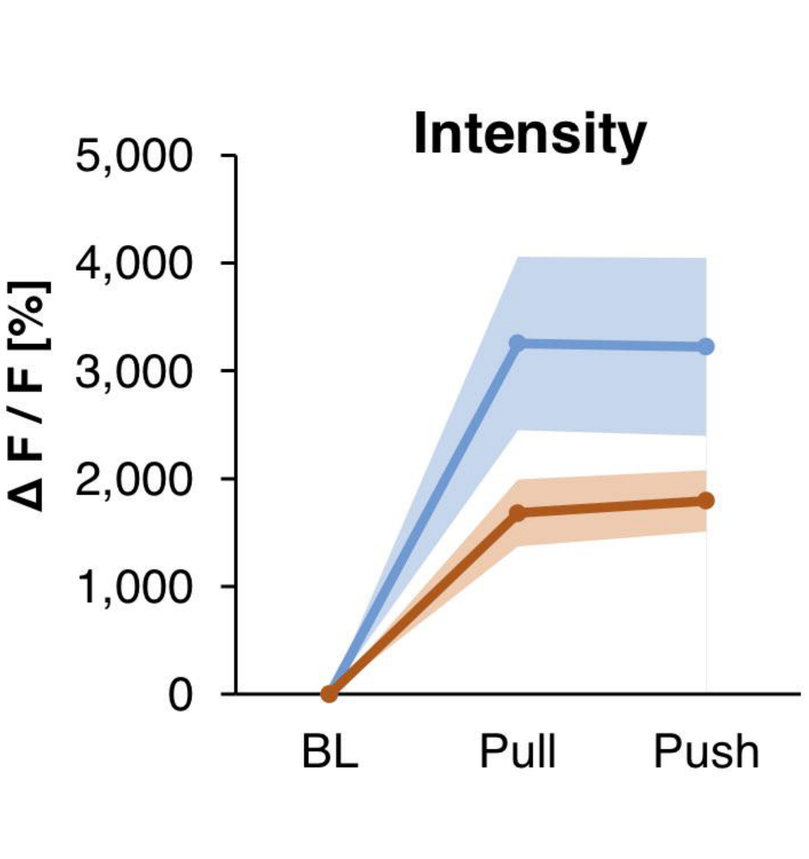

bioRxiv preprint doi: https://doi.org/10.1101/498980; this version posted December 17, 2018. The copyright holder for this preprint (which was not certified by peer review) is the author/funder. All rights reserved. No reuse allowed without permission.

A

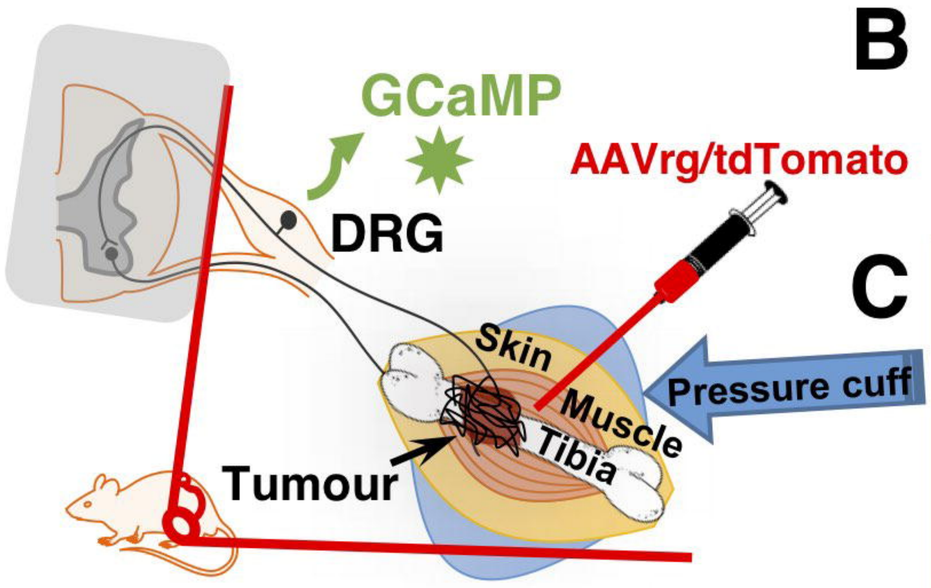

B

Number of cells (number of animals)	Sham	CIBP	Sum
Total (GCaMP+)	757 (9)	1750 (10)	2507 (19)
Muscle (tdTomato+)	14 (3)	42 (5)	56 (8)

C

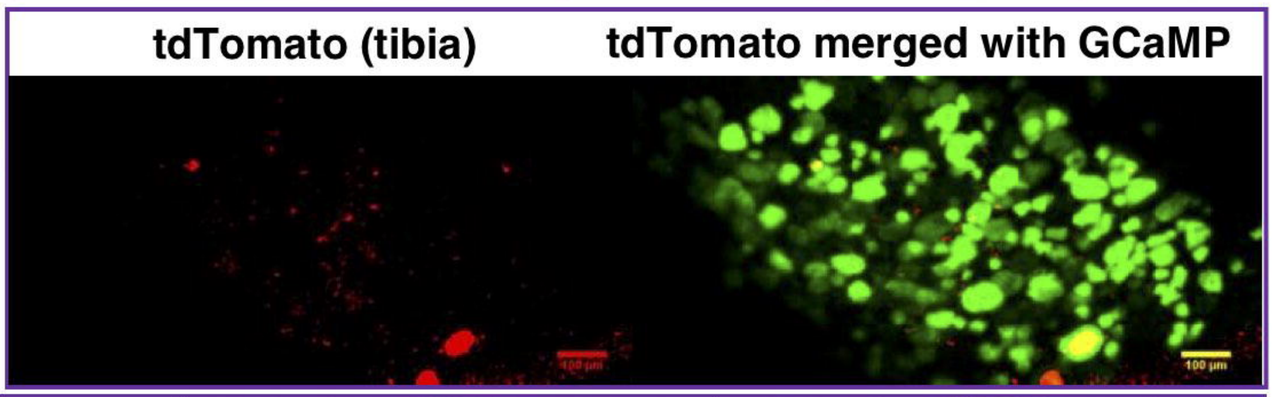

D

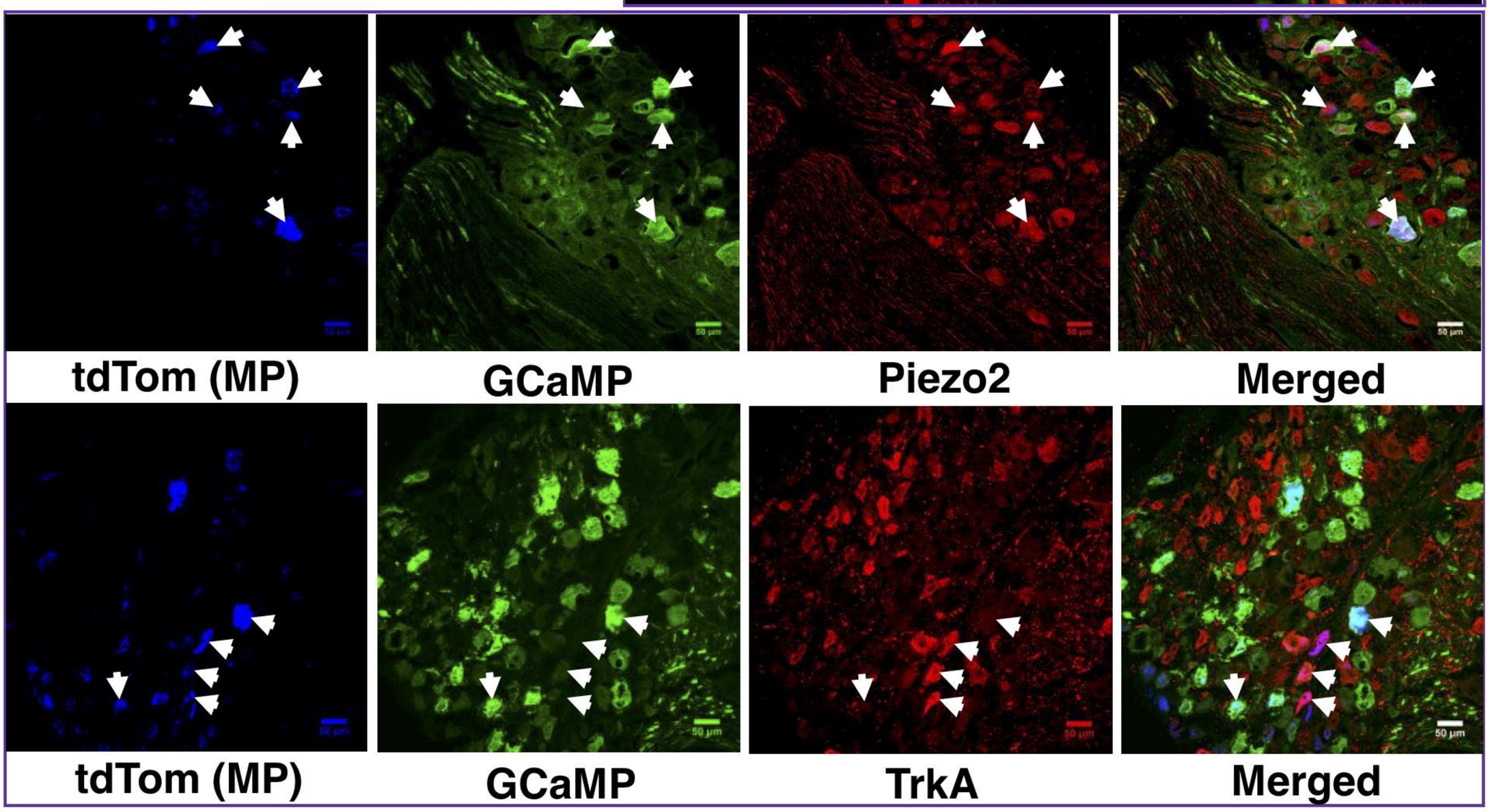

E

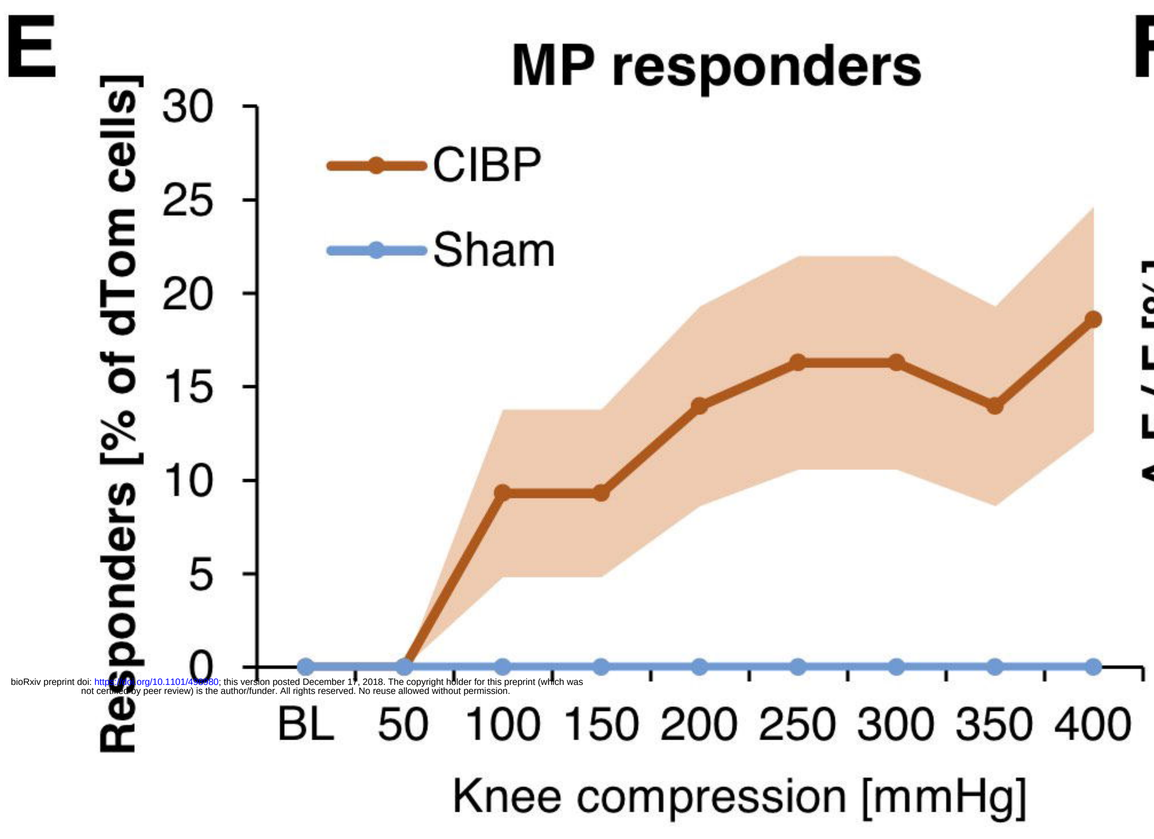

F

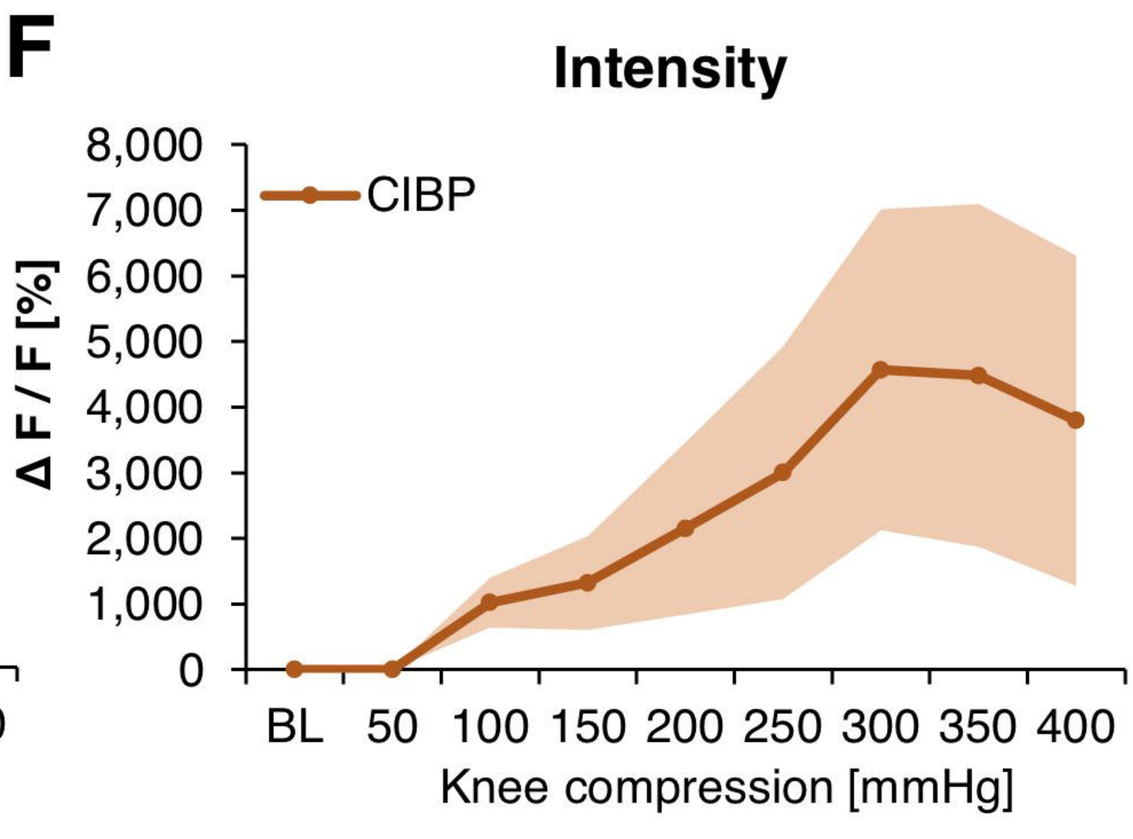

bioRxiv preprint doi: https://doi.org/10.1101/494880; this version posted December 17, 2018. The copyright holder for this preprint (which was not certified by peer review) is the author/funder. All rights reserved. No reuse allowed without permission.

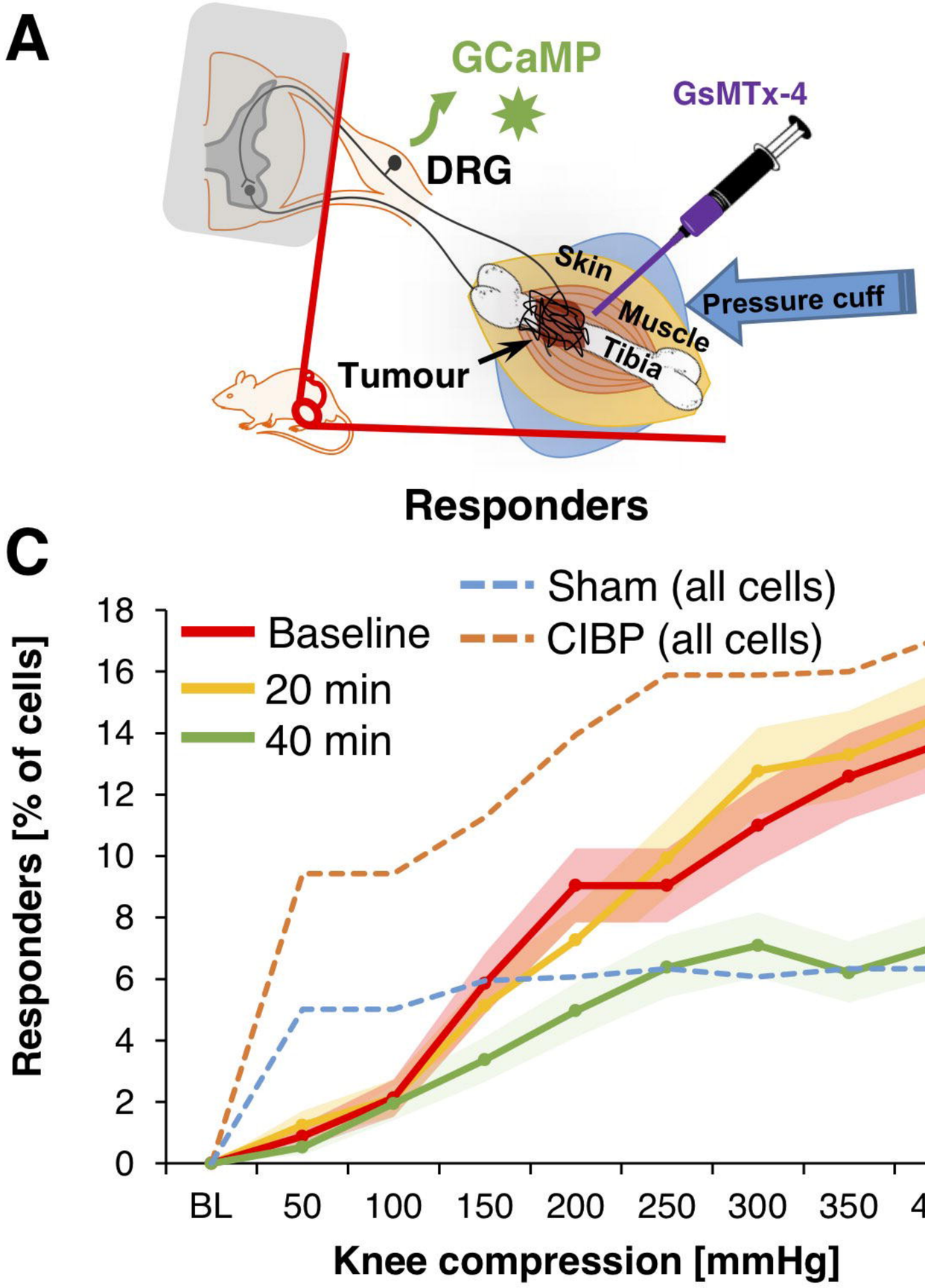

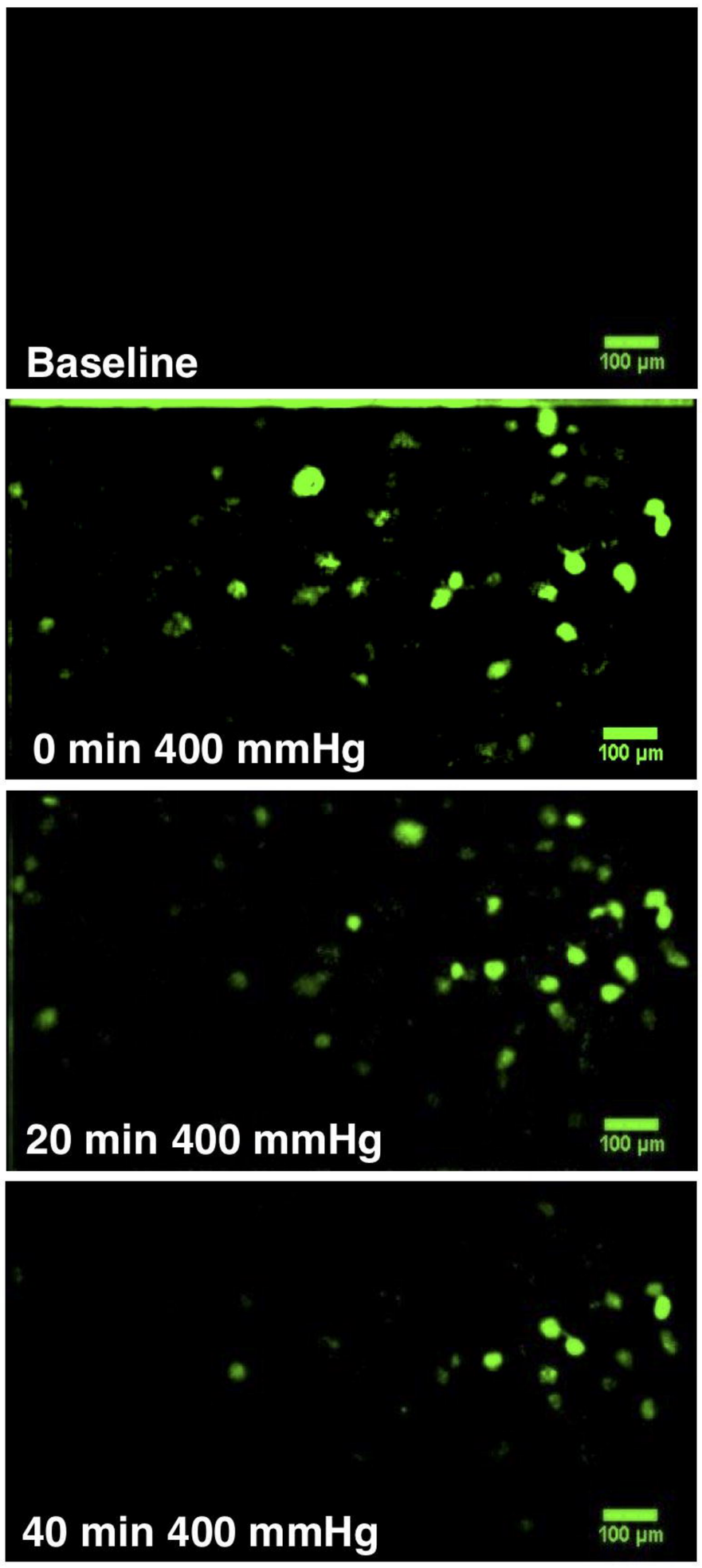

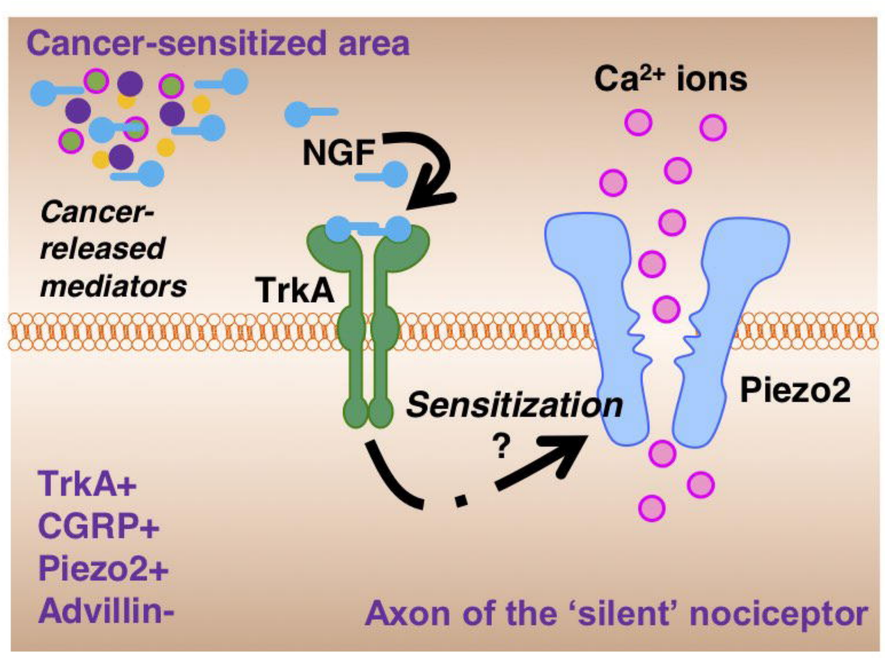

bioRxiv preprint doi: https://doi.org/10.1101/498980; this version posted December 17, 2018. The copyright holder for this preprint (which was not certified by peer review) is the author/funder. All rights reserved. No reuse allowed without permission.